



CHALMERS
UNIVERSITY OF TECHNOLOGY



A comparison between low-cost and professional RTK equipment under forest conditions

Master's thesis in Master Programme Wireless, Photonics and Space Engineering

YIQING WAN

DEPARTMENT OF SPACE, EARTH AND ENVIRONMENT

CHALMERS UNIVERSITY OF TECHNOLOGY

Gothenburg, Sweden 2024

www.chalmers.se

MASTER'S THESIS 2024

A comparison between low-cost and professional RTK equipment under forest conditions

YIQING WAN



CHALMERS
UNIVERSITY OF TECHNOLOGY

Department of Space, Earth and Environment
CHALMERS UNIVERSITY OF TECHNOLOGY
Gothenburg, Sweden 2024

A comparison between low-cost and professional RTK equipment under forest conditions
YIQING WAN

© YIQING WAN, 2024.

Supervisor: Oscar Isoz, Researcher at RISE Research Institutes of Sweden
Supervisor: Per-Olof Hedekvist, Senior Scientist at RISE Research Institutes of Sweden
Examiner: Jan Johansson, Adjunct Professor of Space Geodesy and Geodynamics, Chalmers University of Technology

Master's Thesis 2024
Department of Space, Earth and Environment
Chalmers University of Technology
SE-412 96 Gothenburg
Telephone +46 31 772 1000

Cover: The u-blox F9P RTK rover (left) in operation and the Leica GS18 network RTK rover (right) on standby at Site E on Day 2 (December 7, 2023).

Typeset in L^AT_EX
Printed by Chalmers Reproservice
Gothenburg, Sweden 2024

A comparison between low-cost and professional RTK equipment under forest conditions

YIQING WAN

Department of Space, Earth and Environment
Chalmers University of Technology

Abstract

Real time kinematic (RTK) is an important differential GNSS positioning method. It is widely used in forestry investigation. Depending on the type of reference station, RTK technique can be divided into traditional RTK and the advanced network RTK. There are also different types of GNSS receivers, for example the low-cost mapping type and the professional surveying type. The surveying type devices tend to have more accurate results, but the price difference between the two types of receivers can be dozens of times, and surveying type receivers are usually too bulky to carry and move around in the forest. Therefore, it is worthwhile to analyze if there are any situations that low-cost traditional RTK devices can achieve a comparable performance as the professional network RTK devices do.

In this project, we compared the performance of a low-cost mapping type receiver, u-blox F9P, with a professional network RTK device, Leica GS18 I. Field measurements were taken in two days in the forests near Gothenburg. Measurements were taken in different percentages of canopy closure, different canopy directions and different tree species. Standard deviations and positional errors of the collected positions were calculated. Variables like dilution of precision (DOP), age of differential (AoD), sky plot and time to fix were also collected.

It is found that the real time correction messages (RTCM) communication range for u-blox was at least 500 m in flat area, but terrain obstacles might reduce the range limit by half. The u-blox device performed bad when the canopy closure was over 50% or 65%, with a positional error of over 50 cm, thus it is not recommended to replace Leica network RTK with u-blox in dense forests. In most cases the standard deviation of Leica was better than that of u-blox. DOP was an important factor that had strong correlations with errors, fix status and cycle slips. Data collection with u-blox should wait for 1~5 minutes after power-on, until DOP becomes lower and stable. AoD is found not much related with the error, but there should not be obvious break with the communication of RTCM. Canopy directions influenced the error but had less impact than canopy closure. The relationship between the error and tree species was not able to be determined.

Keywords: GNSS, real time kinematic, network RTK, forest, canopy closure, dilution of precision, age of differential.

Acknowledgements

I would like to express many thanks to my supervisor Oscar Isoz, for giving me many ideas and inspirations over the past half year. He helped me a lot with measurements (especially Leica network RTK measurements), materials and devices preparation, transportation to the measurement sites, etc.

Many thanks to my examiner Professor Jan Johansson, for teaching me a lot of important knowledge in the related fields, answering my questions and pointing out what should be improved in the project.

I would like to thank co-supervisor Per-Olof Hedekvist for giving important suggestions on the project and the thesis writing. Thanks to Erik Lindvall for teaching us the operation of the Leica network RTK device. Thanks to RISE Research Institutes of Sweden for providing this thesis topic, providing the test devices and reimbursing related expenses.

I would like to thank Chalmers University of Technology for providing me with a safe, free and equal environment to study and live. The motto "Avancez!" always shines.

I would like to express many thanks to my father Liming Wan, my mother Faxiu Li, my grandma Nüxiang Zhang and other family members for always supporting me and fully funding me to study in Sweden.

Finally, I would like to thank myself for making it all the way here, arriving at the destination of this Master program.

Yiqing Wan, Gothenburg, February 2024

List of Acronyms

Below is the list of acronyms that have been used throughout this thesis listed in alphabetical order:

AoD	Age of Differential
APC	Antenna Phase Center
ARP	Antenna Reference Point
BPSK	Binary Phase Shift Keying
C/A-Code	Coarse/Acquisition Code
CDMA	Code-Division Multiple Access
CNR	Carrier-to-Noise Ratio
CNSA	China National Space Administration
DGNSS	Differential GNSS
ECEF	Earth-Centered, Earth-Fixed
EGNOS	European Geostationary Navigation Overlay Service
ESA	European Space Agency
FDMA	Frequency-Division Multiple Access
HDOP	Horizontal Dilution of Precision
HEO	Highly Elliptical Orbit
ISM	Industrial, Scientific and Medical
ITRF	International Terrestrial Reference Frame
GEO	Geosynchronous Equatorial Orbit (Geostationary Orbit)
GNSS	Global Navigation Satellite System
GPS	Global Positioning System
GSO	Geosynchronous Orbit
JAXA	Japan Aerospace Exploration Agency
LR	Long Range
MEO	Medium Earth Orbit
MSL	Mean Sea Level
MSM	Multiple Signal Messages
NavIC	Navigation with Indian Constellation
NMEA	National Marine Electronics Association
NRTK	Network RTK
NTRIP	Networked Transport of RTCM via Internet Protocol
P-Code	Precision Code
PDOP	Position Dilution of Precision

PRN	Pseudo-Random Noise
PVT	Position, Velocity and Time
QZSS	Quasi-Zenith Satellite System
RTCM	Real Time Correction Message (or Radio Technical Commission for Maritime Services)
RTK	Real-Time Kinematic
SBAS	Satellite-Based Augmentation System
SD	Standard Deviation
svid	Space Vehicle Identifier
VDOP	Vertical Dilution of Precision
WGS 84	World Geodetic System 1984
ZHD	Zenith Hydrostatic Delay
ZWD	Zenith Wet Delay

Contents

List of Acronyms	ix
1 Introduction	1
1.1 Backgrounds	1
1.2 Aim	2
1.3 Limitations	3
1.4 Thesis outline	3
2 Theory	5
2.1 GNSS systems and signals	5
2.1.1 GNSS systems	5
2.1.1.1 GPS	5
2.1.1.2 GLONASS	5
2.1.1.3 Galileo	6
2.1.1.4 Beidou	6
2.1.1.5 QZSS	6
2.1.1.6 SBAS and EGNOS	6
2.1.2 Signal plans of GNSS systems	7
2.2 Basic principles of satellite positioning	8
2.2.1 Pseudorange measurement	9
2.2.2 Carrier Phase measurement	10
2.2.3 Doppler measurement	11
2.2.4 Differential GNSS	11
2.3 Real-time kinematic (RTK) technique	12
2.3.1 RTK basic principles	12
2.3.2 Real time correction messages (RTCM)	13
2.3.3 Network RTK and SWEPOS	14
2.4 Reference frames	16
2.4.1 WGS 84 and SWEREF 99	16
2.4.2 Height Coordinates	17
3 Methods	19
3.1 Test device	19
3.1.1 Low-cost RTK device: Arduisimple u-blox simpleRTK2B	19
3.1.2 Professional device: Leica network RTK rover	20
3.1.3 Cable connections and pre-settings	20

3.2	Test sites	21
3.3	GNSS Messages and its parsing	22
3.3.1	GNSS Messages	22
3.3.1.1	NMEA Messages	22
3.3.1.2	UBX Messages	23
3.3.2	Parsing messages via Pygnssutils	24
3.3.3	Monitoring through u-center	24
3.3.4	Data collected by Leica NRTK	25
3.4	Data analysis methods	25
3.4.1	Canopy closure analysis	25
3.4.2	Evaluating number and distribution of satellites	26
3.4.2.1	Carrier-noise ratio (CNR)	26
3.4.2.2	Dilution of precision (DOP)	27
3.4.3	Evaluating error, deviation and correlation	27
3.4.3.1	Error of position	27
3.4.3.2	Standard deviation	28
3.4.3.3	Pearson correlation coefficient	28
3.4.3.4	Spearman's rank correlation coefficient	29
3.4.4	Other items evaluated	29
3.4.4.1	Time to a carrier phase fix	29
3.4.4.2	Age of differential	30
4	Measurements and Results	31
4.1	Pretest: RTCM range test	31
4.2	Test on Day 1 (November 1)	32
4.2.1	Test site choosing and settings of base station	32
4.2.2	Detailed method for collection	34
4.2.3	Test Results Analysis	35
4.2.3.1	Canopy closure and CNR of satellites	35
4.2.3.2	Carrier phase solution, stand deviation and error of position	36
4.2.3.3	RTCM and AoD	39
4.2.3.4	DOP	41
4.2.4	Analysis Summary	42
4.3	Test on Day 2 (December 7)	43
4.3.1	Test site choosing and settings of base station	43
4.3.2	Detailed method for collection	43
4.3.3	Test Results Analysis	46
4.3.3.1	Canopy closure and CNR of satellites	46
4.3.3.2	Time to fix and Carrier phase solution	47
4.3.3.3	Standard deviation and error of position	48
4.3.3.4	RTCM and AoD	49
4.3.3.5	DOP	50
4.3.4	Analysis Summary	53
4.4	Correlation Analysis	54
5	Conclusions	57

5.1	Conclusions	57
5.2	Future works	59
	Bibliography	61
A	Figures of measured positions varying with time at each site	I
B	Sky plot of GNSS satellites at each site	VII

1

Introduction

1.1 Backgrounds

Positioning and navigation using Global Navigation Satellite Systems (GNSS) are making important contributions to modern society. In forestry investigation, it is often required to use GNSS techniques to position the trees precisely, in order to make it more convenient for further works like investigating, planting, logging or monitoring the health condition. Ever since 1970s, the GNSS family has been growing up with more satellites and more constellations. The number of GNSS satellites increased much and positioning results become more accurate. On the other hand, differential methods are taken to mitigate errors like clock bias and atmospheric delay. RTK (Real-time kinematic) technique is an important differential GNSS method. Traditional RTK requires a base station to send correction messages to the rover(s) in real time, while network RTK retrieves correction messages based on existed permanent reference stations through the Internet. RTK technique has been widely analyzed and applied in forestry investigation [1–5].

Table 1.1: Comparison of 3 types of GNSS receivers [6–8].

Usage / Types	Recreation	Mapping	Surveying
Accuracy ¹ (in open areas)	3 - 20 m	< 2 m	< 1 cm
Accuracy ¹ (in the forest)		2 - 5 m	< 1 m
Price ¹	< \$600	\$600 - \$2000	> \$10000
Typical product	Smartphone, GPS watch	u-blox F9P	Leica GS18

¹ Based on both the references and Internet searches in 2024.

GNSS receiver systems can roughly be divided into three different categories depending on their capability, i.e. systems for applications such as recreation, mapping and professional surveying. Arranged from low-cost to professional and expensive, a comparison of their accuracy and price is listed in Table 1.1. State-of-the-art GNSS receiving systems like Trimble and Leica have excellent capabilities. However, these receivers are usually quite bulky to carry in the forest and are very expensive. For example, the Leica network RTK device we obtained weighs several kilograms and costs over €20,000. Therefore, in some situations, we would like a lighter and lower-cost system. Arduosimple simpleRTK2B kit is a kind of low-cost RTK system based on a u-blox F9P receiver. As a GNSS system for mapping, it costs only about €700 for both a base station and a rover, with a weight of only 230 g. With RTK applied,

the device is also possible to reach an accuracy of centimeter level. Therefore, it is worthwhile to analyze if and how our low-cost RTK device can achieve a comparable performance to a professional one in the forest, and compare their performance in different forest canopy situations.

In forestry investigation, the tree canopy is a specific error source to analyze. It obstructs the satellite signals and decreases their CNR, as well as causing multipath effect. GNSS devices used for mapping can be four times as accurate in a post-thinning forests as in a pre-thinning one, and the error direction may change [9]. The combination of different GNSS systems (multi-GNSS) gives better result, especially with Galileo in Europe or with geostationary satellites (in SBAS systems) [3, 4]. However, another study showed that for recreation type GNSS receivers in mobile phones, no obvious relationship between the accuracy and the number of frequencies or constellations used are found, and each receiver should be evaluated individually [8]. A study comparing a u-blox F9P device with a receiver for surveying and a high-density LiDAR showed that tree height, elevation and aspect of ground and canopy surface, tree density and slope are the most important factors that influence the performance of this mapping type receiver [5]. Cycle slips, multipath effect and direct signal blockages are also found to have much influence on mapping type and surveying type GNSS receivers [10, 11].

Article [6] reported no significant relationship between the performance and temperature, humidity, atmospheric pressure and wind speed during a one-year's continuous measurement with a recreation type receiver. Study [12] analyzed a mapping type receiver and suggested that holding position of the receiver provides weak to moderate influence to the results. They also found that the relationship is weak between the performance and the atmospheric variables and the season (given the same canopy closure). Some studies showed that the error was affected by the species of trees, but some other studies only found weak relationships [2, 12].

1.2 Aim

In this work, we should evaluate the performance and applicability of u-blox low-cost RTK device in different forest environments, for example, different percentages of canopy closure, different canopy directions and different tree species. We should find out a place that contains the above variety kinds of canopies for our test. The performance of low-cost RTK should be compared with the professional network RTK device under the same conditions. Variables like positional errors, standard deviations, sky visibility, signal quality from satellites, quality of communication with the base station should be collected and compared, as well as the terrain in the line-of-sight to the base station and the time it takes to achieve a fix with an acceptable accuracy. Factors that were proved to be of less relevance in the former studies, like temperature and wind speed, are not needed to be considered.

Finally, we should be able to make recommendations for the circumstances in which

the performance of the low-cost RTK device is good enough to replace the professional NRTK receiver, so that the receiver could be cheaper, more capable and easier to move in the forest. We should be able to come up with a simple but stable test setup that can apply the u-blox RTK kit to real use, including power supply, data logging, hardware and software setup, etc. With a simple setup, the cost of the system can be cut down to one-thirtieth of the cost of the professional device and the device can fit in a backpack.

1.3 Limitations

There are a few limitations to our measurements. The test places are limited, because it is hard to cover all the canopy conditions that may arise in industrial applications. Due to the time limit, we will only test the u-blox RTK kit, but there may also be other low-cost testing devices that are comparable with surveying type devices. We are not going to test other kinds of low-cost devices in this project. The project has a time limit and it is not possible to evaluate the exact same position before and after logging work.

1.4 Thesis outline

Chapter 2 explains basic theory of GNSS systems, satellite positioning principles, traditional RTK and network RTK. Different reference systems involved in different methods are also discussed. Chapter 3 introduces our test devices, the structure and parsing of the collected data and explains the parameters that are collected and compared in data processing. Chapter 4 provides detailed test site description, measurement procedure and results. There were two measurement days, in which the results and the influencing factors were quite different. Therefore, results from the two measurement days are analyzed respectively. The performance between the two devices are compared, and correlation analysis are made to investigate the factors that affects the performance. Finally, in chapter 5, a summary of the test results is shown and some suggestions are made on the circumstances under which a low-cost RTK device is applicable to replace a professional network RTK. Future work outlooks are also discussed.

2

Theory

2.1 GNSS systems and signals

2.1.1 GNSS systems

Global Navigation Satellite System (GNSS) is a collective name for different satellite positioning systems worldwide. At present, there are 4 GNSS systems providing service covering the entire Earth: Global Positioning System (GPS) by the USA, GLObal NAVigation Satellite System (GLONASS) by Russia, Galileo by the European Union and Beidou by China. There are also a few regional GNSS systems that mainly provide service in the regions of their own countries, for example the Quasi-Zenith Satellite System (QZSS) by Japan and Indian Regional Navigation Satellite System (NavIC) by India.

2.1.1.1 GPS

GPS was the first global satellite positioning system that came into use. Owned by the US government and operated by the United States Air Force, GPS has just celebrated its 50 years anniversary since the program was first funded. The first GPS satellite was launched to the orbit in 1978 and the constellation was completed in 1993 with 24 satellites. After that, the US continuously maintained the system, replaced old satellites with new ones and added more satellites for densification or backup. GPS uses medium Earth orbit (MEO) with an altitude of 20,200 km. Currently, there are 32 operational GPS satellites in the orbits [13].

2.1.1.2 GLONASS

GLONASS was built by the former USSR since the first satellite was launched in 1982 and is now operated by Russia. Completed in 1996 with 24 satellites in the constellation, GLONASS was then once declined to only operates 7 available satellites in 2001. In the 21st century, Russia increased the funding to maintain GLONASS and launched new generation satellites. GLONASS is also using MEO orbits. The GLONASS system has restored to 26 operational satellites as of Feb 2024. Apart from MEO satellites, GLONASS is also going to launch Tundra orbit satellites in the future, so that they can stay longer in high latitude areas like Russia [14].

2.1.1.3 Galileo

Galileo was built by the European Union and ESA, aiming at high-precision positioning service primarily for civilian use independent from GPS and GLONASS. It also has a better availability, accuracy and reliability than GPS nowadays. It was first launched in 2011 and came into use in 2016. Similar to GPS and GLONASS, Galileo satellites are also following MEO orbits. The number of Galileo satellites was 23 as of May 2023, but the complete constellation will contain 30 satellites in the future [15].

2.1.1.4 Beidou

Beidou was built by China National Space Administration (CNSA) and was initially the regional GNSS system of China since 2000. After 3 generations of iteration, Beidou realized a global coverage since 2018 and the constellation was completed in 2020. The 3rd generation Beidou system contains not only 24 MEO satellites, but also 3 geosynchronous orbit (GSO) satellites and 3 geostationary orbit (GEO) ones [16]. The participation of GSO and GEO satellites leads to a denser distribution in Asia-Pacific area.

2.1.1.5 QZSS

QZSS is a Japanese regional GNSS system and is operated by Japan Aerospace Exploration Agency (JAXA). It was initially considered as an augmentation system based on GPS, which has the same channel frequencies, and are highly compatible with each other [17]. There are now 3 QZSS satellites in highly elliptical orbit (HEO), guaranteeing that there is always at least 1 QZSS satellite at over 60° elevation in Japan. There is also a GEO QZSS satellite parked at 127°E [18]. In Sweden, one of the QZSS satellites can sometimes be observed at a low elevation in the northeast direction.

2.1.1.6 SBAS and EGNOS

Satellite-based augmentation system (SBAS) can also help and improve the performance of GNSS positioning. The European Space Agency launched an SBAS service called the European Geostationary Navigation Overlay Service (EGNOS). In EGNOS system, correction messages like ionospheric delay, ephemeris error, satellite clock error are collected by on-ground reference stations in Europe. They are sent to geostationary satellites and are then broadcast to the service area, which covers most parts of Europe. GNSS receivers receive SBAS messages from those GEO satellites and make corrections to GNSS measurements [19].

In Sweden, it is only available to receive SBAS service from EGNOS. At present, there are only 2 available EGNOS GEO satellites, one is at 31.5°E with a PRN number of S123; the other is at 5.5°E with a PRN of S136. They are in the southern

sky of Gothenburg with an elevation of 24° and we will meet both of them in the sky plots of our tests later. In addition, other countries including the USA, Russia, China, Japan and India also have their own SBAS systems covering their regions.

2.1.2 Signal plans of GNSS systems

GNSS systems use different channels to send messages. The channels used in our test are listed in Table 2.1. The frequencies are all in L-band, thus many of them have a prefix "L".

Table 2.1: Channel frequencies of GNSS constellations used by our low-cost RTK device (u-blox F9P) and professional NRTK device (Leica) [20].

Constellation	Channel Name	Nominal Carrier Frequency	u-blox F9P	Leica
GPS	L1 C/A	1575.42 MHz	×	×
	L2C	1227.60 MHz	×	×
	L5	1176.45 MHz		×
GLONASS	L1	1598.0625–1605.3750 MHz	×	×
	L2	1242.9375–1251.6875 MHz	×	×
	L3	1202.025 MHz		×
Galileo	E5a	1176.45 MHz		×
	E5b	1207.14 MHz	×	×
	E6	1278.75 MHz		×
	E1 (L1)	1575.42 MHz	×	×
Beidou	B1I	1561.098 MHz	×	×
	B1C	1575.42 MHz		×
	B2I	1207.14 MHz	×	×
	B2a	1176.45 MHz		×
	B3I	1268.52 MHz		×
QZSS	L1 C/A	1575.42 MHz	×	×
	L2C	1227.60 MHz	×	×
	L5	1176.45 MHz		×
EGNOS SBAS	L1	1575.42 MHz	×	×

Code division multiple access (CDMA) is used in GPS to distinguish between different satellites. Signal from satellites are in pseudo-random noise (PRN) codes. PRN codes are BPSK sinusoidal signals, which are unique for each satellite. The table of GNSS system IDs, PRN numbers and satellite names displayed in u-center are listed in Table 2.2. For GPS, on the L1 channel there are the coarse/acquisition code (C/A-code) with a PRN repeating period of 1 ms, the precision code (P-code) with a period of 7 days, and the military codes (M-code) which is never repeated as far as we know. However, P-code is usually encrypted (as "Y-code") and only for authorized users, and M-code is only for military applications, thus what we are going to receive and process from L1 are only the C/A code. On L2 of GPS, our device is collecting L2-CL signals (CL means Civil Long) with a length of 1.5 s, but

L2 is also providing P(Y)-code and M-code. The bandwidth of L1 and L2 of GPS are 24 MHz and 22 MHz respectively. Similarly, Galileo, Beidou and QZSS are also using CDMA signals.

On the other hand, GLONASS is the only GNSS system that (initially) uses frequency division multiple access (FDMA). On L1 and L2, each GLONASS band is divided into 14 sub-bands with bandwidths of 562.5 kHz or 437.3 kHz respectively. Different satellites are using the same code, but different sub-bands to communicate. However, GLONASS signals are changing significantly with new generation satellites since CDMA is also put into use in the new L3 band. The latest GLONASS-K2 satellite launched in August 2023 has already been testing to broadcast CDMA signals in all of the three bands [21].

Table 2.2: GNSS system IDs and satellite PRN rules, in which svid stands for space vehicle identifier. GNSS system IDs and svids of tracked satellites can be obtained from NMEA GNGSV messages.

GNSS System ID	Range of svid	Constellation	Satellite number (PRN number)	NMEA message name prefix
1	1 - 32	GPS	G(svid)	GP-
1	33 - 64	SBAS	S(svid + 87)	GP-
2	65 - 96	GLONASS	R(svid - 64)	GL-
3	1 - 36	Galileo	E(svid)	GA-
4	1 - 63	Beidou	B(svid)	GB-
5	1 - 10	QZSS	Q(svid)	GQ-

2.2 Basic principles of satellite positioning

The basis of GNSS positioning is the ranging between GNSS satellites and the receiver. For a receiver, there are four important parameters to be measured by satellites in the GNSS system: x (latitude), y (longitude), z (altitude) and t (time). Each GNSS satellite has its individual position in an orbital plane roughly 20000 km above the Earth surface. The satellite position data are continuously broadcast to the users. When messages of time and ephemeris are sent to the receiver, the precise positions of the satellites and the time-of-flight of the signals are known. If errors in time and signal delays are ignored, when T is the time the satellite transmits the signal, t is the time the receiver receives it and c be the speed of light in a vacuum, the range R would be

$$R = c(t - T) \quad (2.1)$$

Simple geometry shows that when the range from the receiver to 3 different satellites are obtained, and the exact coordinates of the satellites (X , Y and Z) are known, the coordinate of the station (x , y and z) can be calculated, as shown in Figure 2.1.

However, this requires that the satellites and the station are in the same time reference frame. For a resolution of 3 m, the error of the time synchronization should be only 10 ns. Therefore, a 4th satellite is needed to correct the offset of time and do the synchronization.

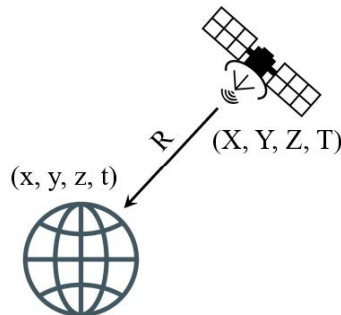


Figure 2.1: The x , y , z and t parameters of a GNSS system.

However, in practice there are much more than 4 satellites. According to experience, at least 40 GNSS satellites are observable under forest conditions if 4 global GNSS systems are all used. The maximum number that can be used for positioning of our u-blox receiver is 32 due to a limit of length of message and bandwidth.

2.2.1 Pseudorange measurement

Pseudorange measurement and carrier phase measurement are two basic methods to measure the distance between the satellite and the receiver. Pseudorange measurement is also called code measurement, because satellite signals are in PRN codes as discussed in section 2.1.2, while the receiver itself also generates the same PRN codes. By comparing its time difference with the received PRN messages, the receiver is able to calculate the range. For a signal travelling from the satellite p to a GNSS receiver k , with a satellite clock time T^p and a receiver clock time t_k , the pseudorange P_k^p will be

$$P_k^p = c(t_k - T^p) \quad (2.2)$$

As its name suggests, pseudorange it is not the actual range in real situations, because many other factors would cause error and should be considered. Atmosphere is a large error source in GNSS measuring. In equation 2.2, the range is calculated only based on the speed of light in vacuum, but in real situation the signal travels through the atmosphere before reaching the receiver, which slows it down and causes delays. There are different delay models for different atmosphere layers.

The signal firstly travels through Earth's nearly 1000-km-thick ionosphere and interacts with the charged ions there. As a result, it losses energy and a ionospheric delay (I_k^p) is induced. The electron density is related with the sun activity, time of the year or day and some other factors, so that it is hard to predict I_k^p . One

example value of ionospheric delay is 5.0 m. However, since the ionospheric delay has the characteristic of dispersion, dual-frequency observation is an effective way to mitigate its error.

After the ionosphere, the signal travels through the stratosphere, whose influence to the signal is little and can be neglected. At last, the signal arrives at the troposphere, which is on average 13-km-thick above the Earth surface. Based on the vapour distribution, the tropospheric delay (Z_k^p) can be further divided into Zenith Hydrostatic Delay (ZHD) and Zenith Wet Delay (ZWD), with the hydrostatic and wet mapping functions m_h and m_w respectively. Assuming ϵ is the elevation angle of the satellite, the total tropospheric delay Z_k^p can be calculated from the mapping function:

$$Z_k^p = \text{ZHD} * m_h(\epsilon) + \text{ZWD} * m_w(\epsilon) \quad (2.3)$$

The typical value at sea level is ZHD = 2.3 m and ZWD = 0 – 0.4 m. There are other models like continued fraction and truncated version, giving different results. Tropospheric delay does not follow dispersion relationship, so dual-frequency method is not applicable. However, it is reported that using default meteorological data is enough to get good result [22].

The clocks also have bias, so clock corrections for the satellite clock ΔT^p and the receiver clock Δt_k are also included into the equation. Finally, we can get the actual range ρ_k^p from equation 2.4 [23].

$$P_k^p = \rho_k^p + (\Delta t_k - \Delta T^p) \cdot c + I_k^p + Z_k^p \quad (2.4)$$

2.2.2 Carrier Phase measurement

Carrier phase measurement uses the phase of the signal to determine the distance. It is used with pseudorange measurement and is more accurate, for it can reach an accuracy of 1/100 of the wavelength (ca. 2 mm). As a sinusoidal signal, the phase received ϕ^p after traveling through the space would have a delay compared with the phase of reference signal ϕ_k at the receiver. By multiplying these two signals in the receiver, the phase of the beat signal Φ_k^p would equal the phase difference between ϕ^p and ϕ_k . Then we can obtain the carrier phase L_k^p :

$$\begin{aligned} L_k^p &= \lambda_0 \Phi_k^p \\ &= c(t_k - T^p) + B_k^p \end{aligned} \quad (2.5)$$

where λ_0 is the nominal wavelength, and the carrier phase bias B_k^p equals

$$B_k^p = \lambda_0(\phi_k - \phi^p - N_k^p) \quad (2.6)$$

In equation 2.6, N_k^p is the phase ambiguity. $\phi_k - \phi^p$ is the fractional part of the phase difference, while N_k^p is an integer describing the how many complete cycles the ground reference signal is ahead of the received signal.

Phase ambiguity is a common source of error, because it is hard for the receiver to determine the precise value. The receiver may guess the value as the number of wavelengths between the receiver and the satellite and keep counting based on this value throughout the measurement, but atmospheric delay and clock bias also affect the phase ambiguity. In some situations, the receiver may lose the solution of phase ambiguity and then define another one. This is called a cycle slip, resulting in a sudden displacement of the positioning result in unit of wavelengths (ca. 20 cm), sometimes happens due to obstructions, low signal-noise ratio, etc. In our measurement, there is an important flag called carrier phase solution (`CarrSoln`). When the state is carrier phase fixed, the phase ambiguity is determined by the receiver; if it is floated, the phase ambiguity has not reached an exact solution yet and can still be improved.

In addition, similar to code measurement, phase measurement also involves ionospheric delay I_k^p and tropospheric delay Z_k^p . Finally the carrier phase measurement model can be written as [23]:

$$L_k^p = \rho_k^p + (\Delta t_k - \Delta T^p) \cdot c - I_k^p + Z_k^p + B_k^p \quad (2.7)$$

2.2.3 Doppler measurement

Doppler effect is the phenomenon that the frequency of the wave changes according to the relative speed between the receiver and the transmitter. Many devices also support Doppler measurement to aid code and phase measurement, because it is an accurate and robust method. As an instantaneous measurement, with certain smoothing algorithms, it can help eliminate the impacts when cycle slips in phase measurement happen [24].

Similar to equations 2.5 and 2.7, the Doppler measurement equation can be written as [25]

$$\lambda_0 D_k^p = \dot{\rho}_k^p + (\dot{\Delta t}_k - \dot{\Delta T}^p) \cdot c - \dot{I}_k^p + \dot{Z}_k^p + \lambda_0 \epsilon_{D_k^p} \quad (2.8)$$

where $\epsilon_{D_k^p}$ is the Doppler ambiguity in integer cycles, and the dots on the parameters represent time derivatives.

2.2.4 Differential GNSS

Differential GNSS (DGNSS) technique uses multiple receivers and satellites to eliminate the errors from ephemeris, clock, ionosphere and troposphere. Consider two receivers j and k observing the same satellite p , as shown in Figure 2.2 (a). Starting from equation 2.7, we can calculate the single differencing phase ΔL_{jk}^p , in which the satellite clock bias τ^p is eliminated:

$$\begin{aligned} L_j^p &= \rho_j^p + (\tau_j - \tau^p) \cdot c - I_j^p + Z_j^p + B_j^p \\ L_k^p &= \rho_k^p + (\tau_k - \tau^p) \cdot c - I_k^p + Z_k^p + B_k^p \end{aligned} \quad (2.9)$$

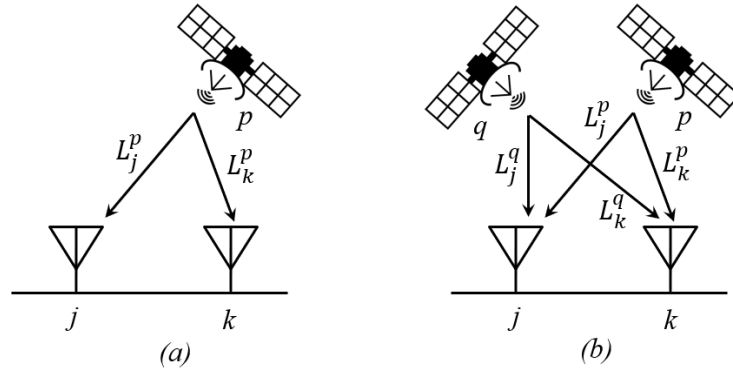


Figure 2.2: Scheme of (a) single differencing and (b) double differencing.

$$\begin{aligned}\Delta L_{jk}^p &= L_j^p - L_k^p \\ &= \Delta\rho_{jk}^p + \Delta\tau_{jk} \cdot c - \Delta I_{jk}^p + \Delta Z_{jk}^p + \Delta B_{jk}^p\end{aligned}\quad (2.10)$$

Similarly, if a second satellite q is introduced as shown in Figure 2.2 (b), it becomes double differencing and the clock bias of the receiver $\Delta\tau_{jk}$ is also eliminated.

$$\begin{aligned}\nabla\Delta L_{jk}^{pq} &= \Delta L_{jk}^p - \Delta L_{jk}^q \\ &= \nabla\Delta\rho_{jk}^{pq} - \nabla\Delta I_{jk}^{pq} + \nabla\Delta Z_{jk}^{pq} + \nabla\Delta B_{jk}^{pq}\end{aligned}\quad (2.11)$$

where $\nabla\Delta B_{jk}^{pq} = -\lambda_0\nabla\Delta N_{jk}^{pq}$ because the carrier phase difference is also eliminated.

When the receivers are close enough to each other and are observing the same satellites, the ionospheric and tropospheric delays can be considered as approximately the same, so $\nabla\Delta I_{jk}^{pq}$ and $\nabla\Delta Z_{jk}^{pq}$ are relatively very small and can also be eliminated from the equation. Finally, equation 2.11 can be further simplified as:

$$L_{jk}^{pq} = \rho_{jk}^{pq} - \lambda_0 N_{jk}^{pq}\quad (2.12)$$

2.3 Real-time kinematic (RTK) technique

2.3.1 RTK basic principles

Real-time kinematic (RTK) positioning is a differential GNSS technique. It is an effective way to provide correction message to GNSS receivers and to enhance the accuracy and efficiency. In traditional RTK technology, apart from the rover(s) that measures the position of interested points, a stationary base station is required. As a differential GNSS method, a relatively precise distance between the base station and the rover can be obtained, thus the precise position of the base station should be known before the measurement, as the error of the position of the base station will be "copied" directly to results of the rover. The base station should broadcast correction message through a radio antenna and they should be received by the rover, as shown in Figure 2.3 (a).

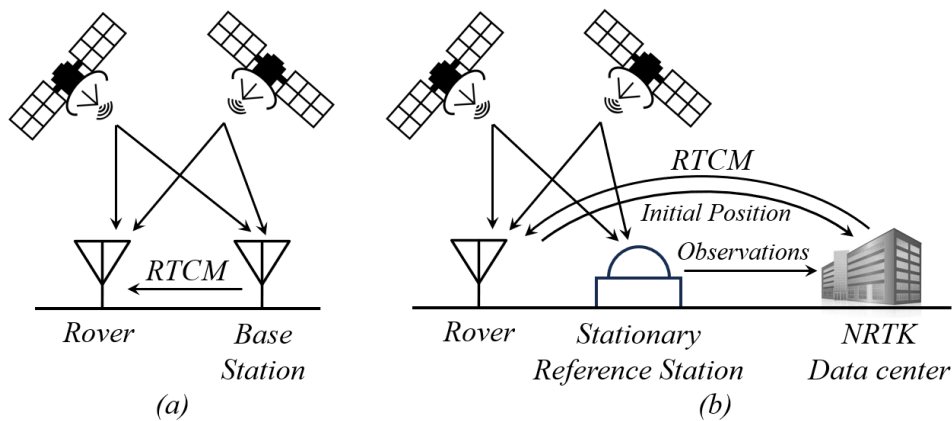


Figure 2.3: Scheme of (a) traditional RTK and (b) network RTK.

The correction messages sent from the base station to the rover are called real time correction messages (RTCM). RTCM contains observational information from the base station, and also the antenna position information, which will be discussed in section 2.3.2.

The accuracy of DGNSS is in decimeter level, while RTK technique reduces error to centimeter level. However, RTK only works when the rover is in a certain range to the base station. The maximum range of traditional RTK is up to 10-20 km, where the ionospheric and tropospheric delays can no longer be neglected. However, it is possible to extend to a long baseline RTK with a range up to 90 km by using certain algorithms, Kalman filters and ambiguity fixing strategies to estimate and mitigate the error from atmosphere, clock and satellite orbit [26]. In addition, the reception of RTCM should be in a good enough quality without obvious interruptions, otherwise the differential GNSS is stopped and the carrier phase ambiguity would have to be estimated again. The maximum range of RTK is also related to the power of the base station's RTCM transmitter antenna, especially for the low-cost ones we are testing.

2.3.2 Real time correction messages (RTCM)

RTCM used in our low-cost traditional RTK measurements are listed in Table 2.3.

Table 2.3: RTCM types available for our low-cost traditional RTK device [27].

RTCM Type	Content
1005	Antenna reference point (ARP) of RTK base station
1074/1084/1094/1124	MSM4 of GPS/GLONASS/Galileo/Beidou
1077/1087/1097/1127	MSM7 of GPS/GLONASS/Galileo/Beidou
1230	GLONASS carrier phase biases information

The first message RTCM 1105 provides the coordinate of antenna reference position (ARP) of our base station to the rover. This coordinate can be inserted by us manually in fixed mode, or it can also be determined within a certain accuracy by the

base station itself in survey-in mode.

In Table 2.3, Multiple Signal Messages (MSM) are information of observations on GNSS satellites. MSM4 contains information about code measurement, phase measurement and CNR measurement. There is an MSM4 RTCM assigned for each global GNSS systems: 1074, 1084, 1094 and 1124. On the basis of MSM4, MSM7 also includes Doppler measurement, and is said to have a higher resolution. They are also assigned to different GNSS systems: 1077, 1087, 1097, 1127.

There are also RTCM 1114 and 1117 corresponding to MSM4 and MSM7 of QZSS system, but they are not available to be enabled in u-center. Moreover, QZSS is a regional system and can only be detected from Sweden seldomly, with a low elevation and a low CNR. Thus, these two messages are not included in our test.

RTCM 1230 is to compensate the inter-frequency carrier phase biases of GLONASS. It is a feature that inter-frequency biases happen in sub-bands of GLONASS's FDMA signals. Following a linear relationship with the frequency of sub-bands, the maximum carrier phase bias of GLONASS can be about 0.35 m [28]. In principle, it is mandatory to use RTCM 1230 together with MSM4 or MSM7, in order to have full interoperability of GLONASS.

However, in u-blox F9P devices, we discover that RTCM 1230 generated by the base station contains no useful information. The RTK system transmits RTCM 1230 indeed, but all the biases information in the message are always 0, which means that they never make any sense to our rover. According to the staff of u-blox, the GLONASS biases are already compensated internally within base station, thus the RTCM 1230 message is empty and there is no need for the rover to process it [29]. They also claimed that it is an industrial practice. However, doubt has been raised whether the internal compensation still works if the rover is not a device from u-blox, because it is known that GLONASS biases are significantly brand-dependent [30]. Since we are using u-blox F9P receiver as both base station and rover, we can simply turn off RTCM 1230 and ignore this problem, but future tests may focus on how u-blox's GLONASS biases compensation works on rovers from other brands.

2.3.3 Network RTK and SWEPOS

Network RTK (NRTK) uses the network of on-ground reference stations, instead of setting up an own base station. In most cases, Internet is required to connect the receiver to NRTK network through NTRIP protocol. The reference stations have relatively very high position accuracy and are being monitored continuously by the central server of NRTK. The initial measured location of the rover is also sent to the central server, where the correction messages are calculated according to the rover's nearby reference stations, and are sent back to the rover. Finally, the rover uses these correction messages to calculate the relative position to the reference station, and hence its absolute position, as what traditional RTK does. The scheme of net-

work RTK is shown in 2.3 (b).

The advantages of NRTK are obvious: it is convenient because only one receiver is required, there is no need for the user to know the precise position of the reference station. Disadvantages are that it needs access to the Internet and an NRTK client account, which is usually not for free. The accuracy decreases with the distance to the nearest reference station, so it is less accurate in area where the density of reference stations is lower.

SWEPOS is a Swedish regional NRTK system run by Lantmäteriet. It contains hundreds of on-ground permanent reference stations, covering all over Sweden, as the map shows in Figure 2.4, and can even connect to some stations in Norway, Finland and Denmark [31]. Reference stations are generating observation information every second, all year round, and all the measured data are sent to and calculated in Gävle, where the data center of SWEPOS is located. As a comparison to the low-cost traditional RTK device, our professional device is able to connect to SWEPOS and retrieve RTCM through the Internet via NTRIP protocol.

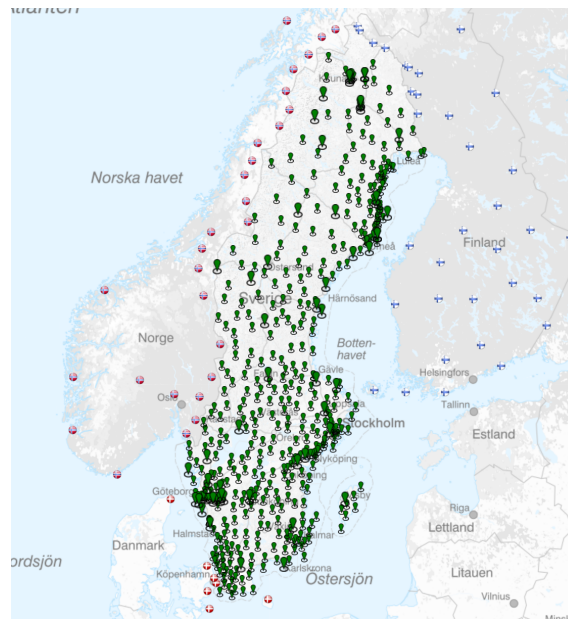


Figure 2.4: Map of SWEPOS permanent reference stations. Cooperated stations from other Nordic countries are also displayed [31].

As of the time of our measurements, SWEPOS is working with GPS, GLONASS and Galileo satellites, but support for Beidou is also being tested since the beginning of 2024 and will come into use in the near future [32]. SWEPOS is also using MSM4 for correction, i.e. 1074, 1084, 1094 and 1124. Apart from MSM4 and RTCM 1105 and 1230, SWEPOS also provides a few other RTCM types, as listed in Table 2.4. It is worth pointing out that those extra RTCM are not available to be generated in the low-cost RTK base station through u-center, otherwise we would rather also open them as a rigorous comparison.

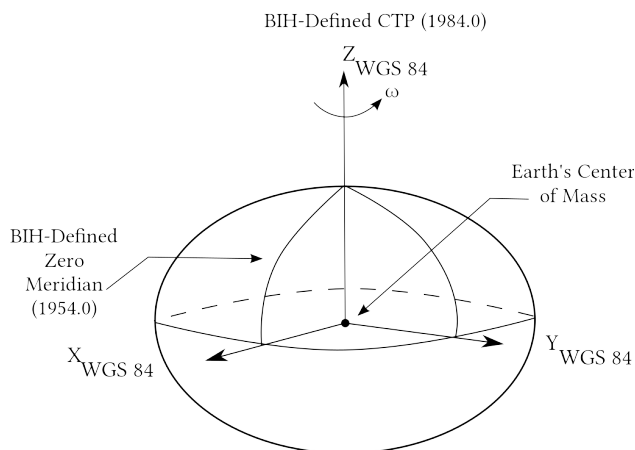
Table 2.4: RTCM types provided by SWEPOS network RTK service [27, 32].

RTCM Type	Content
1005	Antenna reference point (ARP) of the reference station
1007	Antenna descriptor (model, station ID, etc)
1030/1031	NRTK Residual Message of GPS/GLONASS
1032	Antenna phase center (APC) of the reference station
1033	Receiver and antenna descriptors
1074/1084/1094/1124	MSM4 of GPS/GLONASS/Galileo/Beidou
1230	GLONASS carrier phase biases information

2.4 Reference frames

2.4.1 WGS 84 and SWEREF 99

WGS 84 (World Geodetic System 1984) is a global reference system developed by the US Department of Defence and used by GPS. It is the default framework of our low-cost u-blox F9P system. The Earth can be abstracted as a reference ellipsoid, while the coordinate origin is set at the mass center of the Earth, as shown in Figure 2.5. A Cartesian coordinate system is used to describe every point on the Earth surface with X , Y and Z in meters. Due to the drift, rotation, deformation and vertical movement of tectonic plates, WGS 84 is a dynamic system. It is being updated along with the tectonic epoch.

**Figure 2.5:** Scheme of ellipsoid and coordination system of WGS 84 [33].

The latest versions of WGS 84 is very close to the International Terrestrial Reference System (ITRF), which is another similar reference frame determined by the International Association of Geodesy. The main difference of ITRF and WGS 84 comes from different numbers and locations of their ground truth stations, while

WGS 84 is continuously aligning with ITRF. The difference between the two systems has been below 10 mm [34], and in recent documents from Lantmäteriet ITRF 2014 and WGS 84 are used interchangeably [35]. Therefore, in our test, they can be considered equivalent, so that relationships and conversion tools between ITRF and SWEREF 99 can also be used as an alternative to WGS 84.

SWEREF 99 is the Swedish national reference system. In Sweden, SWEREF is updated regularly, instead of WGS 84. SWEREF 99 is determined with the help of 21 class-A SWEPOS permanent stations in Sweden and some cooperated stations abroad (see Figure 2.4). The measured data of network RTK from SWEPOS are in the SWEREF 99 frame. Because SWEREF is continuously using the ITRF tectonic epoch 1989.0, concerning the tectonic movement, the difference between SWEREF 99 and WGS 84 has reached 7-8 dm and is still increasing. Reference [35] introduces the detailed method of the conversion from ITRF 2014 to SWEREF 99, the main idea is to do matrix works and Helmert transformations regarding the tectonic rotations and deformations during the different epochs that the frameworks are applying to. However, it is not necessary for us to go through all these calculations, because websites like Lantmäteriet provide coordinate conversion functions between WGS 84 and SWEREF 99 [36, 37], which will be used by us to convert the coordinate of the reference point. A matlab program is also used in our data processing in order to convert the coordinates of WGS 84 into SWEREF 99 [38], so that the two kinds of devices are in the same reference system.

It is worth pointing out that SWEREF 99 is using transverse Mercator projection, therefore the X , Y , H in SWEREF 99 is totally different from X , Y , Z in WGS 84. X and Y in SWEREF represent longitude (easting) and latitude (northing) in meters. X is measured from the 15° E of Greenwich, which is roughly the central longitude of Sweden, with a value of 500 000 m, while Y is measured from the equator since 0 m. H represents the height above mean sea level. In the following content, unless otherwise specified, X , Y are always coordinates in SWEREF 99 instead of WGS 84, and H is always the height above mean sea level (H_{msl}), because the coordinates we used in the measurements are all converted into SWEREF 99.

2.4.2 Height Coordinates

Geoid is a model of the Earth based on the mean sea level and their imaginary extension over land. Since the Earth is not a standard ellipsoid, the gravity field is variable in different places, so the geoid is irregular. Geoid height N is used to describe the height difference between the geoid and the ellipsoid surface. On the basis of geoid, the height above mean sea level H_{msl} is the difference between the ground surface and the geoid, as shown in Figure 2.6. However, in GNSS applications, the receiver usually provides the height above the ellipsoid h rather than H_{msl} . Therefore it is required to calculate H_{msl} by subtracting the local geoid:

$$H_{msl} = h - N \quad (2.13)$$

The geoid height in model SWEN17_RH2000, which is adapted to SWEREF 99,

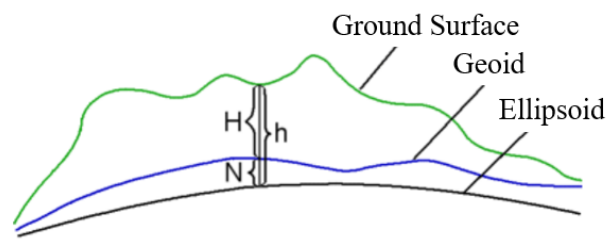


Figure 2.6: Geoid height N , ellipsoid height h and height above mean sea level H .

can be retrieved from Lantmäteriet's website [39] when SWEREF 99 longitude and latitude are given. In Gothenburg area, the geoid height N is typically about 35~36 m.

3

Methods

3.1 Test device

3.1.1 Low-cost RTK device: Ardusimple u-blox simpleRTK2B

Arduimple simpleRTK2B starter kit is the low-cost RTK device used in this study. The GNSS receiver of the kit is the widely used ZED-F9P receiver from u-blox, so this test kit will be referred to as "u-blox" in the following contents. As Figure 3.1 shows, the kit contains two identical receiver sets, each set contains a simpleRTK2B boards with a u-blox ZED-F9P-04B receiver, a u-blox ANN-MB-00 dual band GNSS antenna, a long range radio module and a radio antenna [40]. One set can be used as the base station, while the other set is the rover.



Figure 3.1: The u-blox simpleRTK2B test kit contains two identical sets of components in the above figure [40]. Starting from the top, clockwise: radio antenna, GNSS antenna, LR radio module, u-blox ZED-F9P receiver board.

The u-blox F9P receiver is said to have an accuracy of 1.5 m when standing alone, and can be below 1 cm if RTK is used, with a maximum range of 35 km from the base station. It is multi-frequency and multi-constellation, covering the frequencies marked in Table 2.1 (L1, L2, E5b, etc). The start-up time is 25 s for the first position, and 35 s for a RTK fix [40]. The update rate in our measurement is 1 Hz.

The LR radio module is used for RTCM data communication between the base station and the rover, one acts as a transmitter and the other is the receiver. It transmits correction signal through the radio antenna at a default baud rate of

115,200 bps and a fixed power of 20 mW. The communication is through 863 - 870 MHz ISM band. It is capable both for point-to-point and point-to-multipoint (if multiple rovers are used). The data sheet claims the range in line-of-sight to be 10 km at ideal condition, 5 km at rural condition and 2 km in cities.

3.1.2 Professional device: Leica network RTK rover

The professional network RTK device in our test is Leica GS18 I GNSS RTK Rover (simply referred to as Leica below), providing surveying-level precision positioning. The device can be mounted on a pole to change the antenna height to e.g. 1.2 m. The weight of Leica is 3.55 kg in total, while the weight of a set of u-blox device is only 230 g. With NRTK, the accuracy is supposed to be 8 mm horizontally and 15 mm vertically. Tilt compensation is available for this device, a 30° tilt of the pole would contribute to a horizontal uncertainty of about 5 mm [20].



Figure 3.2: Leica GS18 I GNSS RTK Rover.

The Leica device not only receives all constellations and frequencies that u-blox receives, but is also possible to receive L5 of GPS and QZSS, L3 of GLONASS, E6 of Galileo and B3 of Beidou. When taking a measurement, the Leica device collects 101 dots of positions each time in a few seconds, and calculate the mean position as the result of the measurement. It uses a 4G antenna to connect to the Internet and to retrieve RTCM for network RTK from SWEPOS. It uses an 11.1 V exchangeable Li-ion battery and the data is logged to a micro-SD card.

3.1.3 Cable connections and pre-settings

The F9P receiver is pre-connected to simpleRTK2B board, which contains UART 1 and UART 2 for serial communications. The LR radio module is a kind of XBee module, which can be connected to UART2 port. Power of the board is supplied by a power bank or a laptop from the "Power+GPS" USB port. This USB port also transmits GNSS messages and can be used to connect to u-center on the laptop. The board itself also provides 3.3 V and 5 V power output through pins.

Sparkfun Open-log [41] is used to log the data. It is a tiny and cheap component using micro-SD card and serial ports. It is connected to UART1 of the F9P receiver board with connecting cable. The TX of F9P is connected to the RX of the open-log, while the RX of F9P is connected to the TX of open-log. The power supply of open-log is from the 5 V output pin on the F9P board. In addition, it is required to connect IOREF in UART1 to power, in order to provide a reference voltage to TX and RX on the board. Here it is connected to the 3.3 V pin on the board. After creating a configuration file in the micro-SD card containing the baud rate and a few other settings, open-log would automatically collect all the messages from F9P after each power-on.

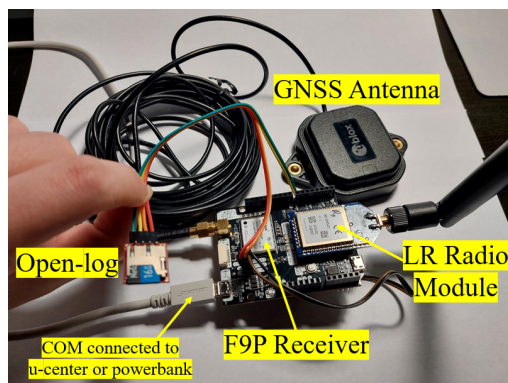


Figure 3.3: An assembled u-blox receiver set.

The base station and the rover are assembled in exactly the same way. The only difference are their configurations of enabling or disabling different kinds of GNSS messages. An assembled receiver set is as shown in Figure 3.3.

3.2 Test sites

The measurements should be taken in the forest or at the boundary of the forest. There should be different densities of forest, and it would be good if different tree species can also be compared. There should be clear forest boundaries in at least south, east and west direction, in order to test the performance if satellite signals from different directions are blocked. There should be a clear sky place to place the base station, better at a higher place, and should not be far away from the above places in the forest.

The tests were mainly taken in two forest area in Greater Gothenburg. The first measurement date (Day 1) was November 1 and the test site was near the north bank of Rådasjön lake in Mölnlycke, southeast of Gothenburg. The second measurement (Day 2) took place on December 7 near Brudaremassen in east Gothenburg. Figure 3.4 shows the locations of these two places and SWEPOS NRTK reference stations nearby. There are SWEPOS reference stations within 2~3 km away from



Figure 3.4: Two test places (red) and SWEPOS stations with in 10 km (blue).

the sites, which is quite close compared with the average density of SWEPOS stations in Sweden. More details of the sites will be described in sections 4.2.1 and 4.3.1.

3.3 GNSS Messages and its parsing

3.3.1 GNSS Messages

3.3.1.1 NMEA Messages

NMEA 0183 or simply NMEA is widely used not only in GNSS applications, but also in marine electronics like sonar, autopilot and other sensors. It is a format defined by the National Marine Electronics Association. It follows ASCII serial communications protocol. There are many different NMEA message types, the types used in our measurements and their brief contents are listed in Table 3.1. They are generated by the receiver, containing many of the most important information that we need about the observable satellites, the position and the accuracy.

Table 3.1: Brief contents of the NMEA messages used in our measurements [42].

Type ¹	Brief content
GxRMC	GNSS specific information (A brief summary of other NMEAs)
GxGNS	Position, fix mode of each constellation, geoid separation
GxGGA	Position, quality indicator (fix mode), geoid separation
GxGSA	DOP and list of active satellites
GxGSV	GNSS satellites in view (details in elevation, azimuth, CNR)
GxGST	Estimated error in position solution

¹ The Gx- in the type names stands for prefix of constellations, which were introduced in Table 2.2, for example GAGSV means the GSV message for Galileo. If the prefix is GN-, it is a message concerning all constellations.

NMEA messages always begin with symbol "\$", followed by the type name and a long list of data field, each separated by a comma, and finally end with a "*" and two-digit hexadecimal checksum. Due to the length limit of NMEA, some of the types may contain multiple messages. The transmit frequency of NMEA can be adjusted by the receiver. In our u-blox receiver, it transmits a whole set of the above messages every second. One example of the structure of NMEA is like:

```
$GNGNS,140400.00,5741.9551720,N,01203.1119027,E,RRRRNN,32,0.50,119.432,38.145,1.0,0000,V*38
```

The meaning can be explained as: UTC time is 14:04:00, latitude is 57°41.9551720' North, longitude is 12°03.1119027' East, fix modes of constellations are "RRRRNN" (RTK fix for GPS, GLONASS, Galileo, Beidou, no fix for QZSS and other constellations), 32 satellites used, HDOP is 0.5, altitude (MSL) is 119.432 m, geoid separation is 38.145 m, age of differential is 1.0 s, reference station ID is 0000, ending and checksum is "V*38".

3.3.1.2 UBX Messages

UBX is u-blox's own protocol for communication between the receiver and a host computer. Data is transferred in 8-bit binary form. It begins with message class and ID, followed by payloads in bytes, and ends up with UBX checksum. Configurations of the receiver are read, sent or changed via UBX messages. RTCM messages are also in UBX format. UBX messages used in our measurement are listed in Table 3.2, in which the last two types are retrieved every second, while other messages are used in pre-settings or the very beginning of the measurements.

Table 3.2: Brief content of the UBX messages used in our measurements [27].

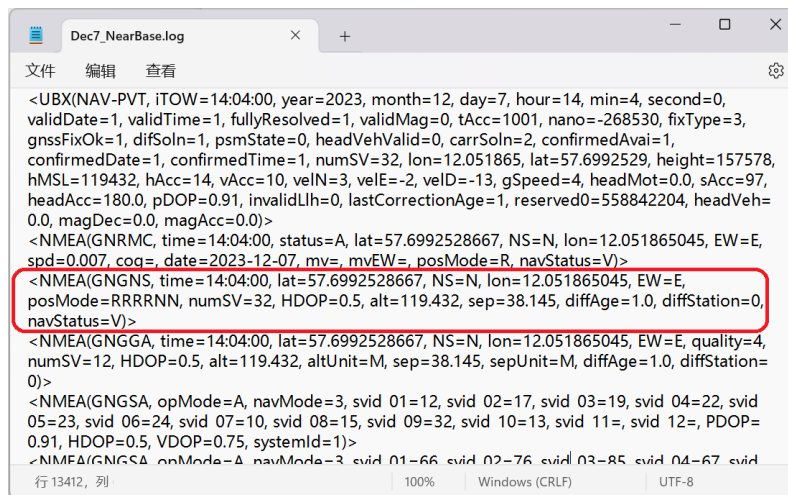
Type	Brief content
UBX-CFG-CFG	Clear, save and load configurations of the receiver
UBX-CFG-MSG	Enable / disable different types of GNSS messages
UBX-CFG-TMODE3	Receiver mode (survey-in / fixed) (base station only)
UBX-CFG-VALGET	Read the configuration items from the receiver
UBX-ACK-ACK	Input message acknowledged
UBX-NAV-PVT	PVT (position, velocity, time) solution
UBX-RXM-RTCM	RTCM messages (Please refer to Table 2.3 and 2.4)

UBX-NAV-PVT is the most important UBX message to analyze. It provides information of time stamp, fix type and mode (No fix, 2D fix or 3D fix), carrier phase fix range solutions (`CarrSoln`), position, velocity and their accuracy, differential correction age (`lastCorrectionAge`), etc. However, there are two fewer significant figures in latitude and longitude values in NAV-PVT than that in NMEA messages, therefore we would always use the position information from NMEA instead, or more

precisely, from GNGGA messages.

3.3.2 Parsing messages via Pygnssutils

Pygnssutils [43] is a powerful python utility library that can read and parse NMEA and UBX messages. All our collected messages are parsed through Pygnssutils into readable information before subsequent processing. An example of parsed message is as shown in Figure 3.5. Note that the message in the red circle is the GNGNS message shown in section 3.3.1.1 after parsing.



```

Dec7_NearBase.log
文件 编辑 查看
<UBX(NAV-PVT, iTOW=14:04:00, year=2023, month=12, day=7, hour=14, min=4, second=0,
validDate=1, validTime=1, fullyResolved=1, validMag=0, tAcc=1001, nano=-268530, fixType=3,
gnssFixOk=1, difSoln=1, psmState=0, headVehValid=0, carrSoln=2, confirmedAvai=1,
confirmedDate=1, confirmedTime=1, numSV=32, lon=12.051865, lat=57.6992529, height=157578,
hMSL=119432, hAcc=14, vAcc=10, velN=3, velE=-2, velD=-13, gSpeed=4, headMot=0.0, sAcc=97,
headAcc=180.0, pDOP=0.91, invalidLlh=0, lastCorrectionAge=1, reserved0=558842204, headVeh=
0.0, magDec=0.0, magAcc=0.0)>
<NMEA(GNRMC, time=14:04:00, status=A, lat=57.6992528667, NS=N, lon=12.051865045, EW=E,
spd=0.007, cog=, date=2023-12-07, mv=, mvEW=, posMode=R, navStatus=V)>
<NMEA(GNGNS, time=14:04:00, lat=57.6992528667, NS=N, lon=12.051865045, EW=E,
posMode=RRRRNN, numSV=32, HDOP=0.5, alt=119.432, sep=38.145, diffAge=1.0, diffStation=0,
navStatus=V)>
<NMEA(GNGGA, time=14:04:00, lat=57.6992528667, NS=N, lon=12.051865045, EW=E, quality=4,
numSV=12, HDOP=0.5, alt=119.432, altUnit=M, sep=38.145, sepUnit=M, diffAge=1.0, diffStation=
0)>
<NMEA(GNGSA, opMode=A, navMode=3, svid 01=12, svid 02=17, svid 03=19, svid 04=22, svid
05=23, svid 06=24, svid 07=10, svid 08=15, svid 09=32, svid 10=13, svid 11=, svid 12=, PDOP=
0.91, HDOP=0.5, VDOP=0.75, systemId=1)>
<NMEA(GNGSA, opMode=A, navMode=3, svid 01=66, svid 02=76, svid 03=85, svid 04=67, svid
行 13412, 列 100% Windows (CRLF) UTF-8

```

Figure 3.5: Readable messages parsed through Pygnssutils.

3.3.3 Monitoring through u-center

u-center is a GNSS evaluation software launched by u-blox. It is well compatible with our u-blox device. It reads the GNSS messages received by the receiver connected to the COM port, and displays information interpreted from the messages. In u-center, there are a lot of functions like setting up the devices, controlling which GNSS messages are enabled or disabled, monitoring the situation of the receiver and satellites, displaying the measured position and its error in real time, recording or replaying GNSS messages and measured results, etc. We used u-center to monitor the rover most of the time when we took measurements, and sometimes recorded the GNSS messages as a backup for recordings from open-log.

However, some errors have been discovered in u-center. For example, it has been found that u-center sometimes misinterprets the PRN number in GNGSA messages, so that it misidentifies some Beidou satellites as from EGNOS. In u-center, the geoid height N matrix provided by u-blox is also not accurate. Therefore, u-center is a useful tool and a source of reference, but it should not always be trusted: NMEA and UBX messages are the most accurate.

3.3.4 Data collected by Leica NRTK

Data collected by Leica device are stored in an micro-SD card. The data can be retrieved in XML format. The data from Leica used in our measurements includes positions, 2D and 3D quality, DOP, number of tracked satellites and used for each point. Tilt compensation info, positional velocity and RTK info are also recorded, but age of differential (AoD) is unfortunately not among the data.

3.4 Data analysis methods

3.4.1 Canopy closure analysis

There are two common parameters to evaluate the forest canopy: canopy cover and canopy closure. As Figure 3.6 [44] shows, canopy cover is the percentage of the ground that are covered by the vertical projection of the tree canopy [45]. Canopy closure can be defined as the solid angle covered by the canopy divided by the solid angle of the whole sky hemisphere (which equals 2π when the ground is absolutely horizontal) viewed from a point. In our measurements, the GNSS antenna can be abstracted as a point, while satellite signals are received from any elevations and azimuths above the ground. Thus canopy closure is a better way to describe the impact of canopy in our measurements.

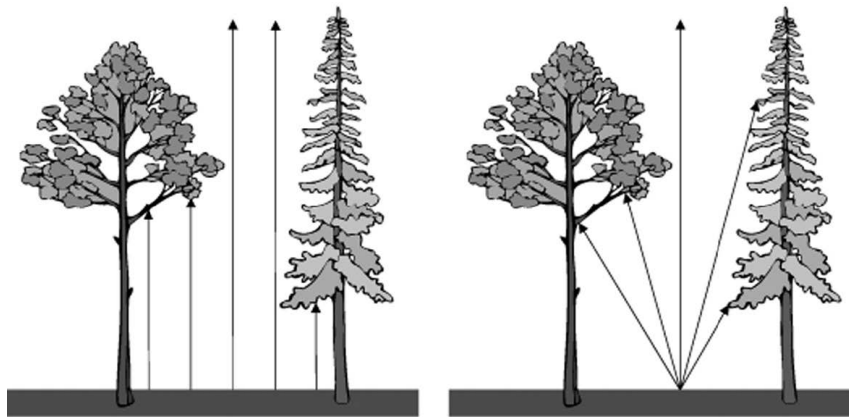


Figure 3.6: Scheme of canopy cover (left) and canopy closure (right) [44].

However, in practice, it is hard to know the exact solid angle that are blocked by canopy from the clear sky. Photos from mobile phone camera can be used to estimate the canopy closure. With a 35 mm equivalent focal length f_{35} of 13 mm in wide-angle lens mode, the field of view of our mobile phone (Samsung A52s) camera can reach about 120° . Considering that the satellites in low elevations make less difference to the test, photos taken by this camera meet the requirement of estimating the canopy closure.

With the camera pointed towards the zenith, sky-view photos are taken carefully as close as possible to our measured points. During the day, areas that are not blocked

by canopy are more highlighted in photos. Our method is to use Adobe® Photoshop® to count the number of highlighted pixels $N_{highlighted}$ and compare it with the total number of pixels N_0 . The highlighted pixels are recognized by selecting a color range of "highlights", with a fuzziness of 20° and a range of 190, but sometimes these parameters varies when brightness and weather conditions are different, so it is still just an estimate. The canopy closure α is then simply:

$$\alpha = 1 - \frac{N_{highlighted}}{N_0} \quad (3.1)$$

One example of the estimated canopy closure is shown in Figure 3.7. The photo is from site "S" in Day 2's measurement. All the area colored green are highlighted pixels picked up by Photoshop and are non-canopy areas. The canopy closure estimated from this photo is 68.30%.

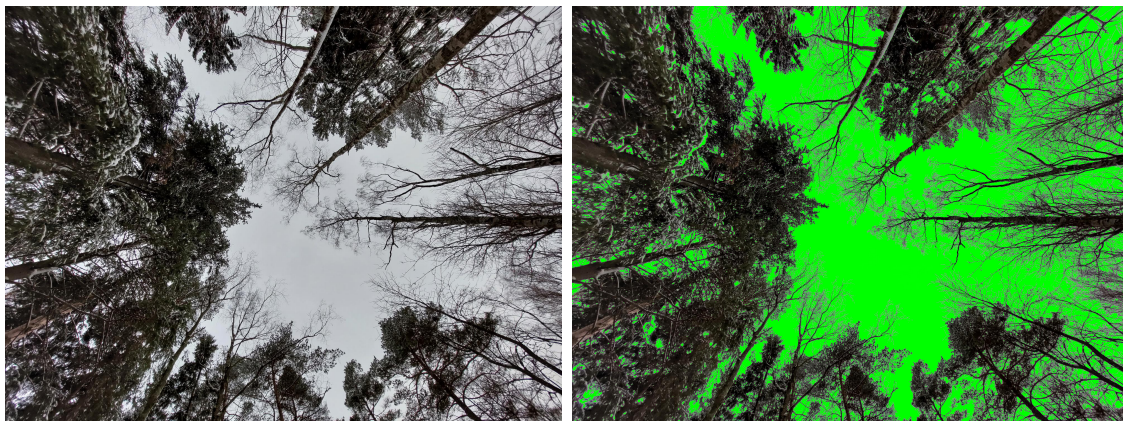


Figure 3.7: An example of sky view (left) and highlighted pixels selected which indicates non-canopy area (right). The canopy closure in this case is 68.30%.

3.4.2 Evaluating number and distribution of satellites

3.4.2.1 Carrier-noise ratio (CNR)

In order to evaluate the satellite signal reception condition, the basic parameter is the carrier-noise ratio (CNR) of the satellite signals. CNR is the ratio of the carrier signal power C received and the noise power N . CNR is often in decibels (dB):

$$\text{CNR}_{dB} = 10 \log_{10}\left(\frac{C}{N}\right) \quad (3.2)$$

A higher CNR means a better reception quality, a higher accuracy and reliability. In GNSS positioning, if the CNR of a satellite signal is better than 40 dB, it is considered to be a very good signal quality. When the CNR is below 25 dB, the possibility of error occurrence is significantly higher [46], thus the use of measurements from those satellites should be avoided. It is commonly required to receive at least 10 satellite signals with a CNR greater than 40 dB at the same time to achieve a good positioning result.

3.4.2.2 Dilution of precision (DOP)

Dilution of precision (DOP) is a dimensionless value reflecting the spatial distribution of GNSS satellites. As Figure 3.8 shows, if satellites are all gathered in a small area, it has a bad distribution and a high DOP; if satellites are distributed in a wide range of azimuth and elevation, it is in a good geometry and has a low DOP.

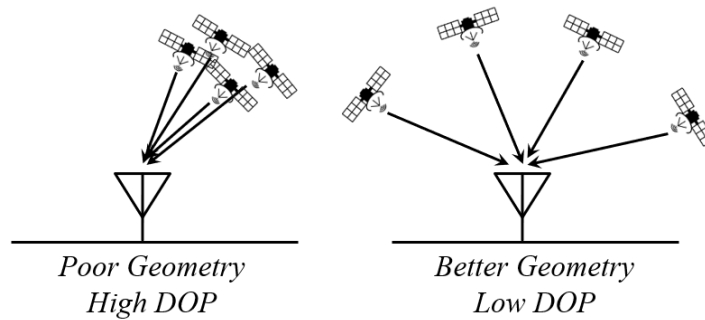


Figure 3.8: Relationship between satellite distribution and DOP.

There are DOP assigned in different dimensions: HDOP for horizontal DOP, VDOP for vertical DOP and TDOP for DOP in time. Combining them will result in PDOP (Position DOP) and GDOP (Geometric DOP):

$$\begin{aligned} PDOP &= \sqrt{HDOP^2 + VDOP^2} \\ GDOP &= \sqrt{HDOP^2 + VDOP^2 + c^2TDOP^2} \end{aligned} \quad (3.3)$$

From the perspective of measurement, the error of the final result is the product of the error of code or phase measurement and the DOP. For example, when the error of code measurement in height is 1 m and VDOP is 2, then the error of the result in height would become 2 m.

DOP is usually calculated by applying matrix inversion to all four-combinations of available satellites and selecting the best ones. At least 4 satellites are there required to calculate a DOP. The criteria for DOP is as follows: <1 for an ideal DOP, 1 - 2 for an excellent DOP, and 2 - 5 for a good one [47].

DOP is related to locations of satellites visible and the CNR of their signals. It is sensitive to obstacles that block the signals. Since the satellites are moving, DOP varies with the change of ephemerides from time to time.

3.4.3 Evaluating error, deviation and correlation

3.4.3.1 Error of position

Error of position is the most intuitive parameter to evaluate the performance of our devices.

For Day 1's measurement, the base station and the site "NearBase" were at a geodesy control point, whose precise position was obtained from Lantmäteriet's website. At this site, error of position was the difference between the measured position and the precise position of the control point. At other sites, the measured distance and angle between our u-blox antenna and the Leica antenna were compared with the result from measuring tape. Note that we only used the average position of u-blox or Leica at each site for comparison, rather than comparing any single point.

For Day 2's test, the test procedure was changed, and we were measuring exactly the same point by u-blox and Leica. In this case, the position difference between u-blox and Leica was directly the positional error between them. The error distance and angle was always calculated from u-blox to Leica, because u-blox was the one we were more interested in. Although this was only the relative error between the two device, but the smaller the error, the more it proved that "our low-cost RTK device can replace the professional NRTK device" was true, because that means we were able to obtain very close positions when using these two devices.

3.4.3.2 Standard deviation

Standard deviation (σ) evaluates the dispersion of data from the mean by calculating the residual. The standard deviation of the set of positions collected at each site is calculated and compared. A larger σ means the data has a larger variance, but it has nothing to do with the absolute error of the data. For a data set of x_1, x_2, \dots, x_n containing n data, The equation of σ_x is:

$$\sigma_x = \sqrt{\frac{\sum_{i=1}^n (x_i - \bar{x})^2}{n}} \quad (3.4)$$

where \bar{x} is the mean value of the data set.

For different dimensions of positioning, the combined standard deviation follows the square root of the sum of squares, e.g., for a data set with easting x , northing y and height h values, the 2D and 3D standard deviation σ_{2D} and σ_{3D} would be

$$\begin{aligned} \sigma_{2D} &= \sqrt{\sigma_x^2 + \sigma_y^2} \\ \sigma_{3D} &= \sqrt{\sigma_x^2 + \sigma_y^2 + \sigma_h^2} \end{aligned} \quad (3.5)$$

3.4.3.3 Pearson correlation coefficient

Pearson correlation is a useful method to investigate if two sets of data follow a linear relationship. For a pair of data sets x and y , The formula for Pearson correlation $r_{x,y}$ is

$$r_{x,y} = \frac{\text{cov}(x, y)}{\sigma_x \sigma_y} = \frac{\sum_{i=1}^n (x_i - \bar{x})(y_i - \bar{y})}{\sqrt{\sum_{i=1}^n (x_i - \bar{x})^2} \sqrt{\sum_{i=1}^n (y_i - \bar{y})^2}} \quad (3.6)$$

where \bar{x} and \bar{y} are mean values of x and y , n is the number of data sets.

r is in a range of $-1 \sim 1$. The closer the absolute value is to 1, the stronger the linear correlation is, and vice versa. If r is positive, the two data sets are in a positive correlation; if r is negative, they are in a negative correlation. The strength criteria of r used in our measurements is as listed in Table 3.3 [48].

Table 3.3: Strength criteria for Pearson correlation coefficient r or Spearman's rank correlation coefficient ρ [48].

$ r $ or $ \rho $	0~0.2	0.2~0.4	0.4~0.7	0.7~0.9	0.9~1
Correlation strength	None	Low	Medium	High	Very high

3.4.3.4 Spearman's rank correlation coefficient

The shortage of Pearson correlation is that it only analyzes the linear relationship. Spearman's rank correlation coefficient ρ is the Pearson coefficient of the rank variables of the data sets. It tests the monotonicity of data relationships regardless of whether they are linear or not. If values in two data sets tend to have similar ranks, $|\rho|$ would be larger. For two sets of data x and y , if their rank variables are $R(X_i)$ and $R(Y_i)$, the formula of $\rho_{x,y}$ is:

$$\rho_{x,y} = 1 - \frac{6 \sum_{i=1}^n d_i^2}{n(n^2 - 1)} \quad (3.7)$$

where $d_i = R(X_i) - R(Y_i)$ and n is the number of data.

The strength criteria of ρ is the same with that of r in Table 3.3.

3.4.4 Other items evaluated

3.4.4.1 Time to a carrier phase fix

Time to a carrier phase fix (or simply time to fix) is the time since the receiver is turned on till its phase ambiguity N is determined and reaches a carrier phase fixed status. Usually, in a floated state, the measured position fluctuates a lot and sometimes experiences cycle slips, while the measured position is much more accurate in a fixed status, therefore time to fix can describe how long time should people wait before the position becomes stable and usable. Time to fix is analyzed from the flag CarrSoln in UBX-NAV-PVT.

However, in some bad conditions the fix state may be lost or it may keep struggling between fixed and floated. Sometimes the position from a later fix is more accurate than the first one, so two kinds of time to fix are examined: Time to the first fix T_{fix0} , and time to a better fix T_{fix} .

Table 3.4: `lastCorrectionAge` values from message UBX-NAV-PVT and AoD time range. All time ranges are left-closed and right-open intervals.

<code>lastCorrectionAge</code> value	0	1	2	3	4	5
AoD time range / s	Not Available	0~1	1~2	2~5	5~10	10~15
6	7	8	9	10	11	≥ 12
15~20	20~30	30~45	45~60	60~90	90~120	≥ 120

3.4.4.2 Age of differential

Last differential correction age, or age of differential (AoD), is the delay between the time the differential correction message is generated and the time that it is received by the rover. Accuracy of the RTK position decreases when AoD becomes longer, because the locations of satellites, the location of the receiver, the condition of atmosphere or other environment variables may have changed when old differential information is used. AoD is related to the base station (or the server if NRTK is used), the receiver and the path of RTCM propagation. A typical good AoD is about 1~2 s. It is suggested to avoid AoD above 15 s, while an AoD of below 5 s would be ideal, contributing to a position error in cm or sub-cm level [49].

In our measurements, AoD is analyzed from the flag `lastCorrectionAge` in message UBX-NAV-PVT. It uses different values to represent AoD time ranges, as listed in Table 3.4.

4

Measurements and Results

4.1 Pretest: RTCM range test

The reception of RTCM messages is a prerequisite for RTK techniques. If RTCM messages are not received by the rover, RTK will not work. Therefore, before our field measurements, it is necessary to have a test on the range that RTCM can travel continuously between the LR radio antennas of the u-blox base station and the rover.

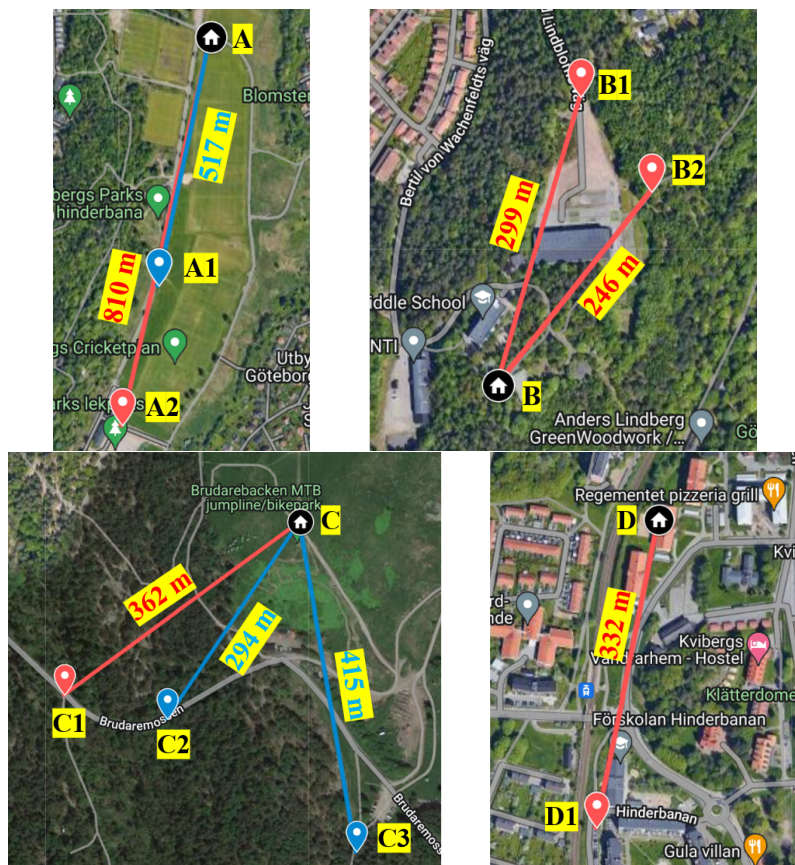


Figure 4.1: RTCM range test. Black home symbols represent the base stations. Red markers and lines indicate that the communication of RTCM was interrupted through these routes, while the blue ones mean the RTCM reception was continuous.

Quick tests were done on flat ground (A), mountains (B, C) and residential areas (D). The RTCM reception situation was read through the status of the LED light

"XBEE>GPS" on the ArduSimple board of u-blox device. When it flashes frequently, it represents that the device is retrieving RTCM messages from the LR antenna continuously. If the LED stays off, the RTCM communication is interrupted. Once the base station was set up, I took the rover and walked or rode away from the base station, and monitored the LED light until it stopped flashing.

The test results are shown in Figure 4.1. In test A, on flat ground, the RTCM was continuous until the range reached 500 m. Then it began to experience some interruptions. It became unable to retrieve RTCM with a range of 800 m. However, in this test, the base station was put directly on the ground. According to the principle of antenna's Fresnel zone, if the base station was mounted at a higher place, the range could be extended.

Test B showed that the base station was quite sensitive to the terrain of the mountains in the line-of-sight to the base station. The base station was placed near the flat top of a hill. The signal was blocked by the convex slope since the top of the slope even if the range was only 250 m from the base station.

In test C, the base station was mounted on the top of a little hill. The hill was higher than the one in test B. For location C1, there were some terrain obstacles in the line-of-sight, so that the signal had a hard time to be received. However, there were fewer obstacles for C2 and C3, so the reception at C2 and C3 was good, although C3 was further away than C1.

In test D, the base station antenna was put out of a window in the second floor of a building. It showed that the RTCM could be blocked by buildings in residential area in a range of only 330 m. In this case, the RTCM signal was blocked by just a little garage house, as there were no other obstacles in the line-of-sight.

From those pretests, some suggestions can be made: Communication of RTCM is quite sensitive to terrain obstacles (when using this kind of LR antenna). It is recommended to mount the base station antenna at a higher place, for example the top of a hill. When there is no obstacle, the RTCM communication would be fluent in a range of at least 500 m, but it can easily be blocked by buildings in a range of 330 m, or obvious terrain obstacles in a range of 250 m.

4.2 Test on Day 1 (November 1)

4.2.1 Test site choosing and settings of base station

Our test on Day 1 (November 1, 2023) was done near the Rådasjön lake. We used a geodetic control point as our reference point to place the base station. The reference point is an iron stud in rock with a small depression in the center, where we could aim our antenna or Leica pole at. Information about the point is shown in Table 4.1, and can also be found on Lantmäteriet website.

Table 4.1: Reference point information and the setting of the base station.

Information	Reference Point	Base Station Setting	Base Station Recorded
ID	7619592	-	-
Reference Frame	SWEREF 99 TM	WGS 84 ECEF	SWEREF 99 TM
X / m	326414.415	3343512.3661	326414.4090
Y / m	6395572.691	716151.2036	6395572.6948
Location uncertainty / m	0.015	-	0.022
Reference System of Height	RH 2000	WGS 84 LLH	RH 2000
Mean Sea Level Height H / m	87.64	-	87.63
Ellipsoid Height h / m	-	125.74	125.74
Height uncertainty / m	0	-	0.01

The reference point is on the top of a high rock with a clear sky. It is the best place to set up the base station, because the precise location of it is already known. This became our first test site and we call it “Near Base”. In order to setup a fixed position for our u-blox base station, we first converted X and Y in SWEREF 99 TM coordination into WGS 84 via the matlab program [38], then insert it to the TMODE3 settings of the u-blox base station kit through u-center.

For the height, in order to set up the base station, it is required to input the ellipsoid height h . Mean sea level height H of the reference station was obtained from Table 4.1. However, u-center was applying its own geoid height N grid matrix, whose exact value is unknown. According to experience, we guessed N to be 38.10 m at the site, therefore the input h became 125.74 m. In later data process, we discovered the actual N value used in u-center at this area was 38.11 m, so 0.01 m was then added back to the height of all data from u-blox. The location information was also output and listed in Table 4.1, which was very close to the given reference point, indicating that the settings in the base station were accurate enough.

Although it did not influence out test, it is worth pointing out that the N grid used by u-center was not accurate (at least in Gothenburg area). From the Lantmäteriet website [39], an precise value of N can be found, which is 35.739 m in our test area.

We chose 4 other sites according to terrain and tree species, as shown in Figure 4.2. Two of them were in birch forest. One of them was on a stump, the other one was on the ground near birches. They were named “Birch (1)” and “Birch (2)”. The third site named “Bank” was on the ground near the bank of the lake, where there was roughly clear sky on the southwest side and some tree canopy on the northeast side. The last one was quite near from Bank, but was in an oak forest. The site was named “Oak” and was on a low rock near oaks.

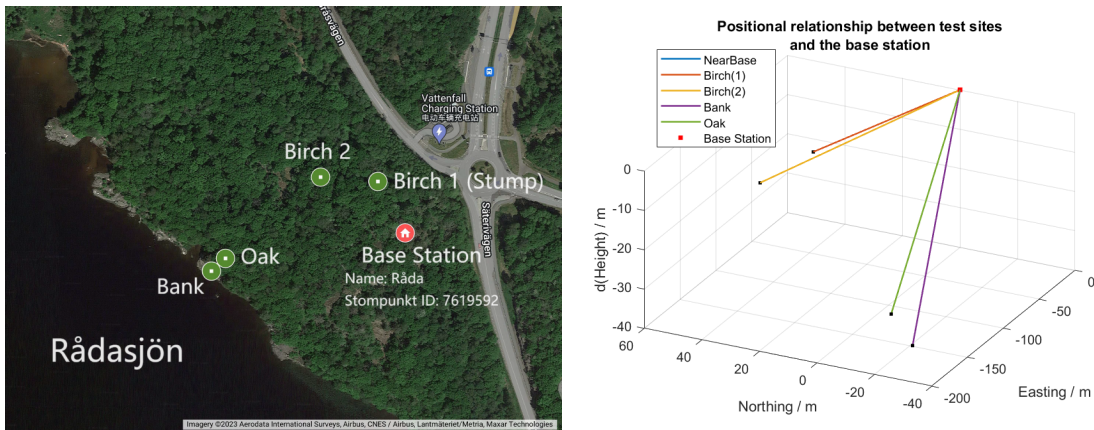


Figure 4.2: Google satellite map and 3D positional relationship plot of our sites. Site "NearBase" is too close and is covered by the marker of the base station.

4.2.2 Detailed method for collection

At Near Base, we firstly aimed the Leica pole directly at the reference point, and collected enough points. Then we put the GNSS antenna of the u-blox base station, whose TMODE3 had been set up, on the center of the reference point. The base station was then kept working, sending RTCM and recording data during the whole test. The base station was always sending 6 RTCM messages each second, which were 1005, 1074, 1084, 1094, 1124 and 1230 (please refer to Table 2.3). The rover was then placed 15 cm north to the reference point, and was about 5.5 cm lower. The distance was adjusted back in later data processing, so that a comparison of absolute error to the reference station could be made. This only applied for Near Base; in other sites, the relative error between the locations of the two devices were compared.

At other sites, we collect data for u-blox and Leica NRTK in roughly the same time. The antennas of u-blox and Leica NRTK were placed close. The distances between the antennas $\Delta 2D_0$ were measured by a roll ruler, and the directions were measured by a compass on mobile phone. However, the compass on mobile phone was quite inaccurate because the reading was changing from time to time. It only showed the general direction. Therefore, the main comparison was just the 2D distance of the antennas.

Other studies suggested that 30~50 fixes per point position were enough for a mapping or recreation type GNSS measurement [6, 12, 50]; increasing the number of position fixes from 10 to 50 at each site did not significantly improve the performance [12]. Therefore, around 30 positions per site were collected by Leica NRTK in our measurements in Day 1. Those points were collected when NRTK was connected, and the reading was stable with a high accuracy (if possible). At the same time, the u-blox rover was also opened and was collecting its data in a frequency of 1 point / second. After the rover had received the RTCM from the base station and reached a fixed state (if possible), we started to record and left it alone for 5 minutes, which would become 300 points.

4.2.3 Test Results Analysis

4.2.3.1 Canopy closure and CNR of satellites

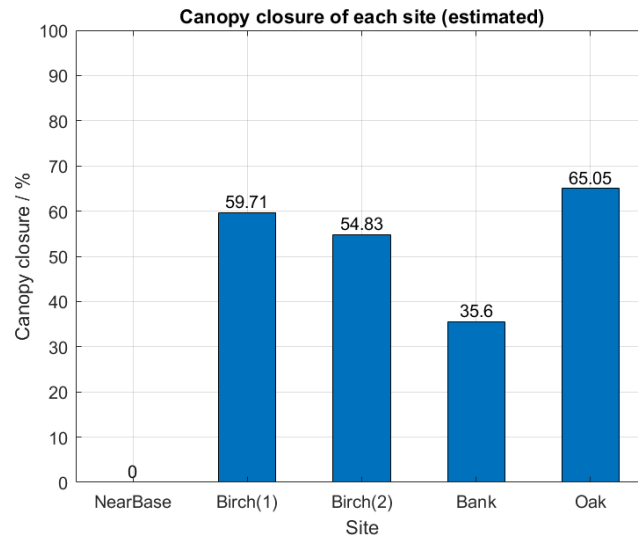


Figure 4.3: Canopy closure of each site.

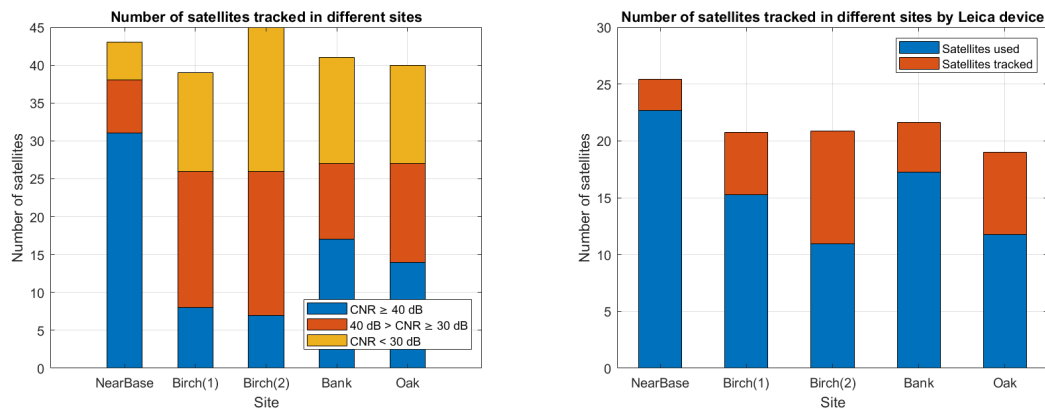


Figure 4.4: Numbers of satellites in different sites tracked by u-blox kit (left) and Leica NRTK (right).

The estimated canopy closure of each site is shown in Figure 4.3. There was a clear sky at Near Base, while at Bank, the southeast half of the sky were empty and the overall closure α was 35.6%. At other sites the canopy were covered in all directions with a closure α between 54% and 65%.

The number of satellites tracked by u-blox and Leica NRTK at each site is shown in Figure 4.4. The sky plots for all sites are shown in Appendix B.

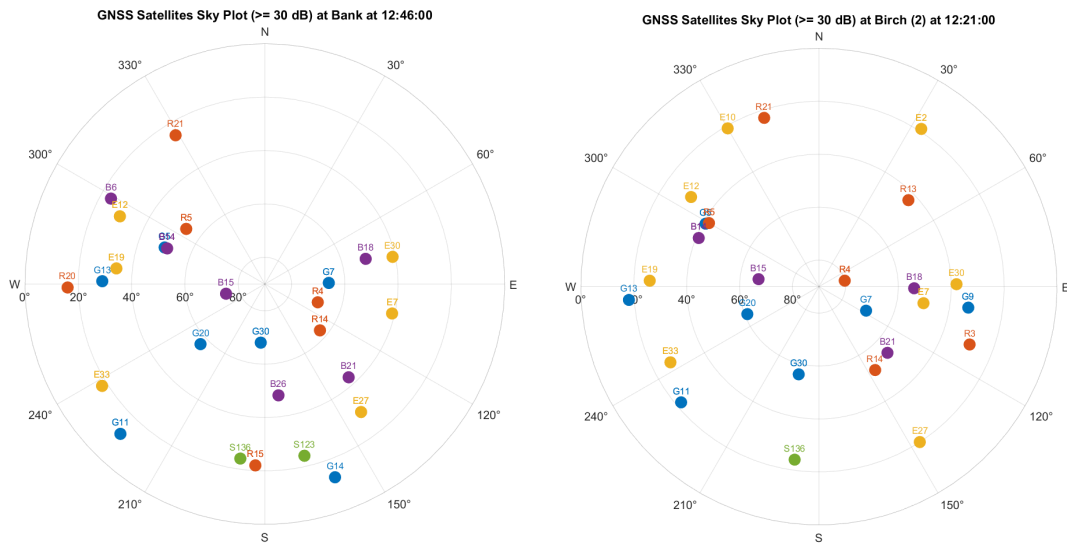


Figure 4.5: Sky plots of satellites whose CNR are better than 30 dB at Bank (left) compared with Birch (2) (right). An empty area at northeast side can be seen.

For u-blox, at Near Base, the number of satellites with a CNR better than 40 dB (N_{40dB}) was 32, which was the best site. At Birch (1) and Birch (2), N_{40dB} were less than 10, which could be identified as a bad visibility. At Bank, there was only tree canopy on the northeast side. As the sky plot in Figure 4.5 shows, there was an obvious blank area in the north and northeast direction. But the total number of satellites was good, with $N_{40dB} = 17$. At Oak, the sky plot was similar to Bank, with $N_{40dB} = 14$.

For Leica NRTK, number of satellites tracked was much less than by u-blox. Except for site Near Base which had more than 25 satellites tracked, the total number at other sites were just around 20, with 10~18 of them used. This was reasonable because Leica NRTK was not using any Beidou satellites.

4.2.3.2 Carrier phase solution, stand deviation and error of position

The test results for satellite visibility, carrier phase solution, stand deviation and positional error of each site are shown in Figures 4.6 - 4.7 and Tables 4.2 - 4.3. Figures for the easting, northing, 2D position and height of the points collected at each site and their detailed changes over time can all be found in Appendix A.

Near Base was the only site that our result could be compared directly with the reference point, whose position was known precisely. After processing the data, the 2D errors of u-blox and Leica NRTK $\Delta 2D_{ref}$ were 0.0091 m and 0.0199 m, while the errors in height ΔH_{ref} were -0.0054 m and -0.0221 m respectively. The standard deviations σ of the dots were less than 0.5 cm for u-blox and about 3 cm for Leica. It seems that the u-blox kit had a better performance in this site, but this is

Table 4.2: Number of points before and after filtering.

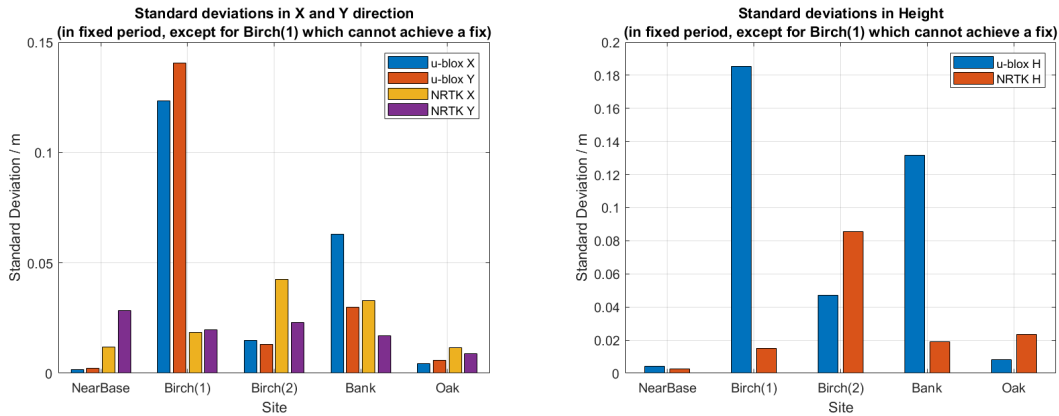
Site	u-blox		Leica NRTK		
	All	In fixed state	All	After filter 1 ¹	After filter 1&2 ²
Near Base	322	322	27	27	27
Birch (1)	Invalid ³	0	33	32	32
Birch (2)	363	39	39	30	19
Bank	357	82	28	27	27
Oak	494	124	21 ⁴	9	9

¹ Filter 1 is to delete dots whose 3D quality are worse than 0.1 m. 3D quality is obtained from Leica's output data.

² Filter 2 is to delete dots which are more than 0.08 m away from the average point.

³ Invalid due to a mistakenly early starting of collection.

⁴ Due to a low battery, less dots were collected at Site Oak.

**Figure 4.6:** Standard deviations σ of u-blox (left) and Leica NRTK (right).**Table 4.3:** Location differences to the reference point Råda at Near Base.

Site	Test Set	ΔX_{ref} / m	ΔY_{ref} / m	ΔH_{ref} / m	$\Delta 2D_{ref}$ / m
Near Base	u-blox	0.0069	-0.0059	-0.0054	0.0091
	Leica NRTK	-0.0176	-0.0092	-0.0221	0.0199

4. Measurements and Results

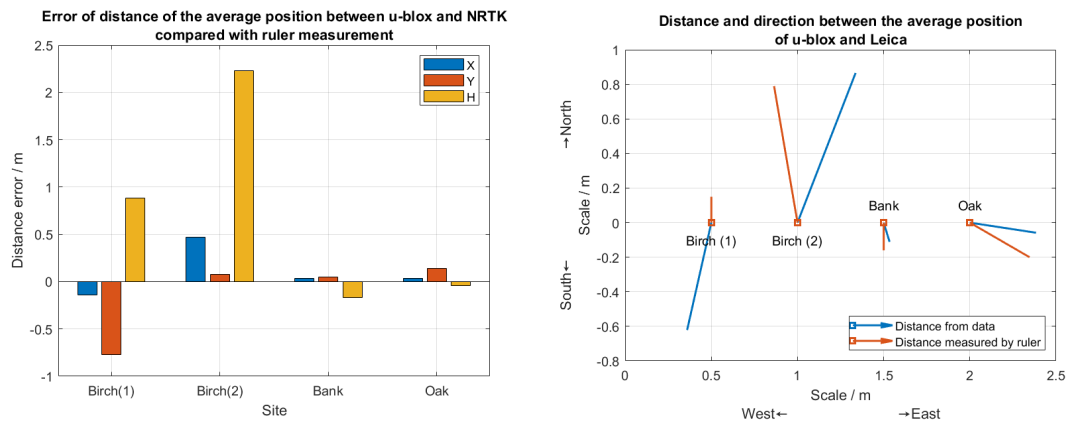


Figure 4.7: Location differences and directions between average locations of u-blox and Leica NRTK ΔX , ΔY and ΔH at the other 4 sites. (Directions are all from u-blox to Leica)

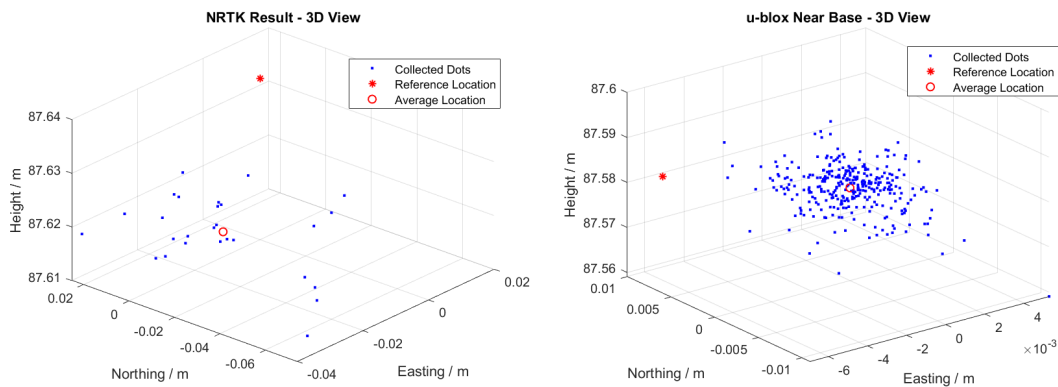


Figure 4.8: 3D plots of all dots at Near Base from Leica NRTK (left) and u-blox (right).

reasonable because it was only 15 cm away from the u-blox base station, while the Leica was only using NRTK correction service, whose nearest reference station was 1.87 km away.

At Birch (1), for u-blox, the position was unstable and never reached a fix during the measurement. σ_{u-blox} increased to $0.1 \sim 0.2$ m, while the σ_{Leica} roughly remains the same as at Near Base. It was likely that u-blox suffered from a poor satellite visibility, while Leica survived. The distance between two kinds of antenna $\Delta 2D_0$ was about 15 cm, but the test result $\Delta 2D$ was 63.71 cm, which was very inaccurate.

At Birch (2), the carrier phase state reached a fix at 12:19:39, but only lasted for about half a minute. Only data after the fix were selected to calculate the standard deviation and the average position. σ_{u-blox} was worse than Near Base but much better than Birch (1). The Leica NRTK, on the other hand, was not as good as at Birch (1). It was a hard time for Leica to collect dots at this site and it sometimes got totally lost of position. After the filters, only 19 of the 39 dots collected were

left. The σ_{Leica} increased a lot as well. $\Delta 2D_0$ was about 158 cm, but test result $\Delta 2D$ was 93.54 cm.

At Bank, the u-blox device was in a fixed state only between 12:45:17 and 12:46:40. Only this relatively stable period was selected to calculate the standard deviation and the average position of u-blox. σ for both devices were worse than Birch (1) but better than Birch (2). For NRTK, only 1 of the dots had a bad 3D quality and was filtered out during the data procession. $\Delta 2D$ was measured to be 11.66 cm when u-blox reached a fix, while the actual value was 16 cm. This value was much better than that of Birch (1) and Birch (2).

At Oak, the u-blox kits reached a fix when we started to record data, but the fixed state was lost between 12:57:28 and 13:03:32. During the period after the latter fix, σ_{u-blox} was than 1 cm in any direction. Leica was still in a bad situation because only 9 of the 21 dots were left after the filters. During the last fix, $\Delta 2D$ was 38.83 cm compared with 40 cm measured by roll ruler. The direction error was 22° . Considering the uncertainty of the compass on mobile phone, this error was quite small.

4.2.3.3 RTCM and AoD

The continuity of RTCM reception can be measured by the average number of RTCM received every second \bar{N}_{RTCM} . The base station sent 6 RTCM messages each second, therefore the range of \bar{N}_{RTCM} was from 0 to 6. The value of \bar{N}_{RTCM} of each site is shown in Figure 4.9.

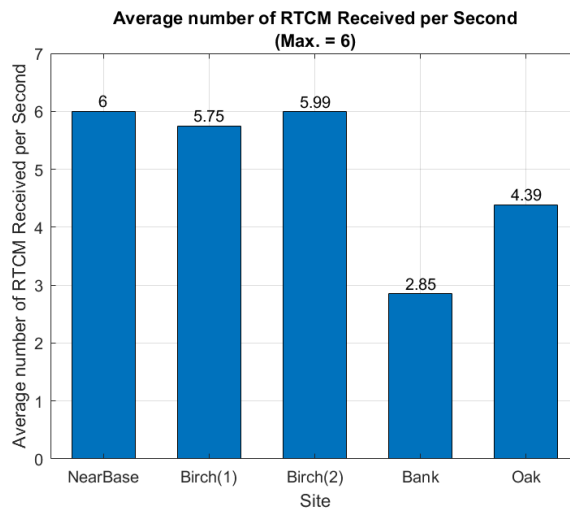


Figure 4.9: \bar{N}_{RTCM} of u-blox at each site on Day 1.

The RTCM reception was quite continuous at Near Base, Birch (1) and Birch (2). The rover received most of the RTCM at those places.

4. Measurements and Results

The RTCM receiving condition at Bank was worse, with less than half of the RTCM received. The site was at the lowest place by the lake, near some rocks on a slope, which might hid our site behind the shadow of the terrain in the line-of-sight to the base station. The RTCM reception was a little bit better than Bank, because the site Oak was just on the top of one of the rocks that blocked the line-of-sight from the base station to Bank.

In Figure 4.10, disruptions and breaks of RTCM reception can be seen clearly. Losing RTCM messages means the rover was not applying RTK technique and was working alone. For example, for site Oak there was an RTCM break between 12:56:22 and 12:58:32, and some little interruption at 13:02. As a result, the u-blox rover lost the fix state at 12:57:28. Then the position was floating for a long time with a range of more than 3 m in easting or northing and 8 m in altitude, until the RTCM resumed. It reached a fix again at 13:03:32, as shown in Figure 4.11.

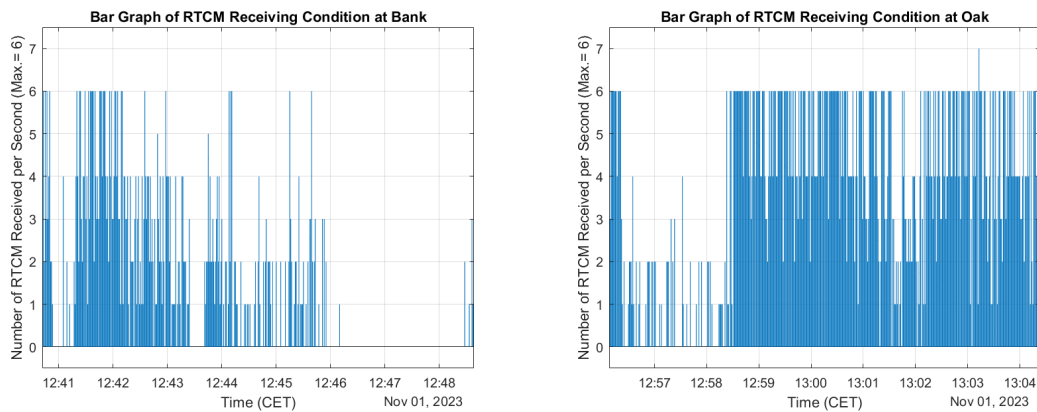


Figure 4.10: Examples of bad RTCM reception: Bank (left) and Oak (right).

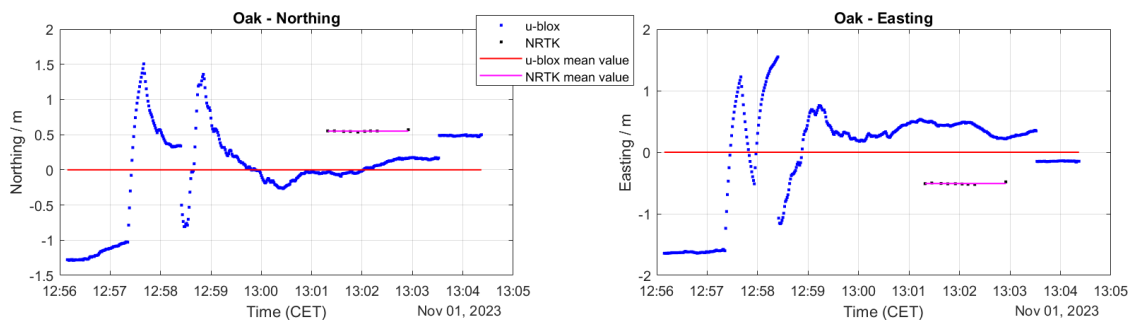


Figure 4.11: Change of the position of site Oak with time. A reflection of poor RTCM reception.

AoD is another way to evaluate the RTCM reception. Mean AoD levels and error bars are shown in Figure 4.12. Similar to \bar{N}_{RTCM} , AoD level was lower (better) at Near Base, Birch (1) and Birch (2), and was higher (worse) at Bank and Oak. The RTCM breaks resulted in high AoDs. For example, the 2-minute break of RTCM at

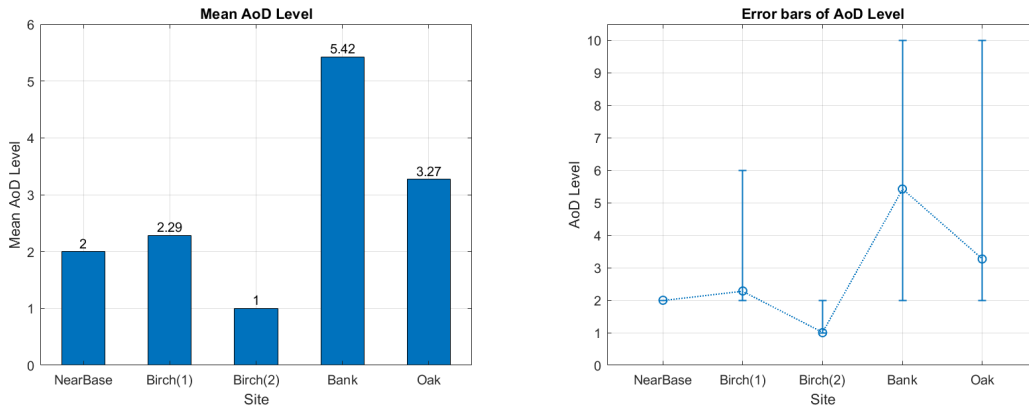


Figure 4.12: Mean AoD level and error bars. For the corresponding relationship between AoD level and time, please refer to Table 3.4.

site Oak caused an AoD of up to level 10 before it became invalid, which indicates the differential message age was 60 ~ 90 s old, as shown in Figure 4.13.

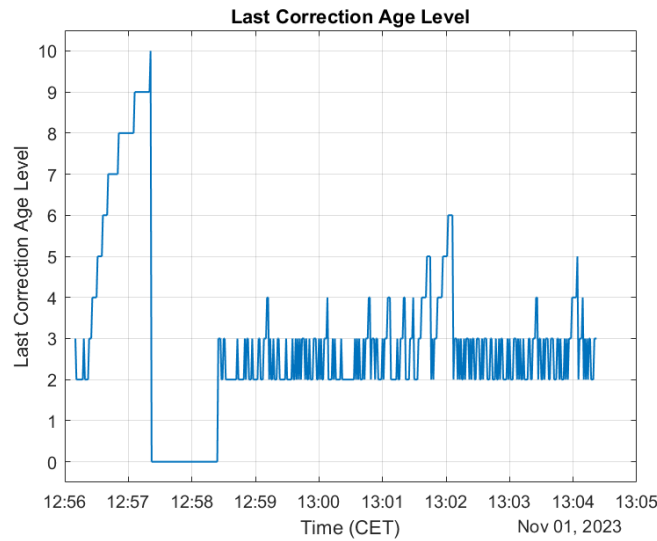


Figure 4.13: AoD level - time plot at site Oak.

However, values of \overline{N}_{RTCM} and AoD level showed different trends with σ and the position error in Day 1's measurement. It indicates that they were not the main contributor to the σ and the position error.

4.2.3.4 DOP

Error bars of horizontal and vertical DOP of each site measured by u-blox and Leica NRTK are shown in Figure 4.14. The DOP to some extent reflected the standard deviation. For u-blox, at Birch (1) and Bank, HDOP and VDOP were larger (especially the maximum value), which corresponded to a larger σ_{2D} and σ_H in these two

sites. Similar situation also happened to Leica NRTK at Birch (2). However, mean or extremum values of DOP was less able to reflect the positional error $\Delta 2D$ or ΔH .

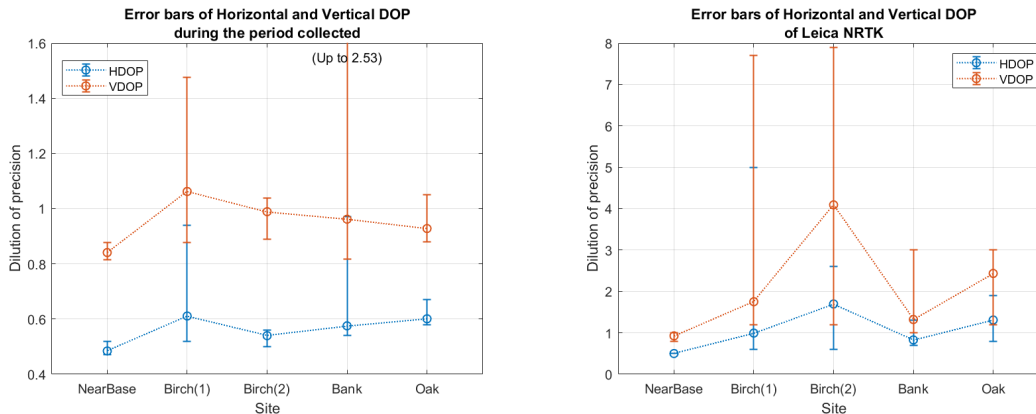


Figure 4.14: Error bars of horizontal and vertical DOP of each site measured by u-blox (left) and Leica NRTK (right).

4.2.4 Analysis Summary

In conclusion of Day 1's measurements, it seems that the low visibility of GNSS satellites was a larger risk to the performance, rather than the receiving smoothness of RTCM. At Birch (1) and Birch (2), the RTCM reception condition was good while the satellite visibility and CNR was poor, resulted in worse $\Delta 2D$ and ΔH . The circumstance at Bank and Oak were opposite, while $\Delta 2D$ and ΔH were better than the former two sites. However, although RTCM is no much needed to be always very continuously, it should be good enough for u-blox to access for RTK, otherwise a very low \overline{N}_{RTCM} or a large AoD would result in a long time to fix T_{fix0} or the lost of a existed fix.

DOP influenced the standard deviation of both u-blox and Leica NRTK horizontally and vertically. The details about how DOP influenced the position in real time will be discussed in the next test date in Section 4.3.3.5.

Canopy closure was positively related to positional error, except for site Oak, whose α was high but both positional error and σ were low. Due to insufficient data volume, it is unknown whether it was by coincidence or contributed by the difference of tree species.

Comparing u-blox and Leica, the performance varied in different sites. When the rover was very close to the base station (within a few cm), u-blox won obviously. Leica performed better at Birch (1) and Bank, but was worse at the other two sites. σ of Leica was higher than that of u-blox in Birch (2) and Oak, and more than half of the collected Leica dots had a bad quality, as listed in Table 4.2. Only at sites Near Base, Bank and Oak could Leica NRTK be replaced by u-blox, with error of

positions $\Delta 2D$ and ΔH less than 15 cm. In the other two sites, the error of positions were over 50 cm in 2D and were 1 to 2 m in altitude.

4.3 Test on Day 2 (December 7)

4.3.1 Test site choosing and settings of base station

In order to collect more data and to test the performance with certain directions covered by canopy, we went to another test place, Brudaremossen, to do further measurements on Day 2 (December 7, 2023). The satellite map of our test sites and photos of canopy condition are all shown in Figure 4.15.

The base station was on the top of a little hill in Brudaremossen. The hill was only covered with low grass, but there were plenty of pine or fir forest around the hill, with an altitude difference of about 20-30 m from the top of the hill to the edge of the forests. In order to put the RTCM transmitting antenna higher, we placed the base station antenna on the top of the left wooden stake of a billboard. The billboard, as shown in the photo "Near Base" of Figure 4.15, was quite sturdy and stable, free from shake when pushed by hands or kicked by feet. It was a nice place to place the base station, because there was a clear sky, and it was about 80 cm higher than the ground, so that the signals from satellites were not affected by the ground, and the transmission of RTCM had a better performance. We also chose a site about 5 meters next to this billboard and marked it as site "Near Base", with also clear sky. The Near Base site would be used to correct the bias of the pre-settings of our base station, which will be mentioned later.

Our other 6 sites are all at or near the edge of the forest, as the 3D plot shows in Figure 4.16. They were mainly in two areas: the west edge and the south edge of the forest. At the west edge, we had a site with canopy on the west side and marked as site "W". Next to site W, we went dozens of meters into the forest. The forest here was not very dense, but did cover all directions, so we picked this site as "Undense". The species of the trees was pine. At the south edge, which was a little bit further, there were 4 test sites. There were sites where canopy is on the south side ("S") or east side ("E"). A site with a canopy denser than site Undense was also chosen as "Dense". In addition, we also found a site on a path, where the canopy was covered on both east and west sides, but the sky was relatively clear at south and north sides. This site was named as "Two sides". The tree species of these 4 sites was fir. The horizontal distances between our sites and the base station on the top were from 150 m (to the west) to 400 m (to the south). The elevation angles from the sites to our base station were in a range of 3.71° - 7.67° .

4.3.2 Detailed method for collection

The position of the base station was measured individually by our Leica device before the test day, and the position had been inserted to the base station before the



Figure 4.15: Google satellite map of our sites at Brudaremassen.

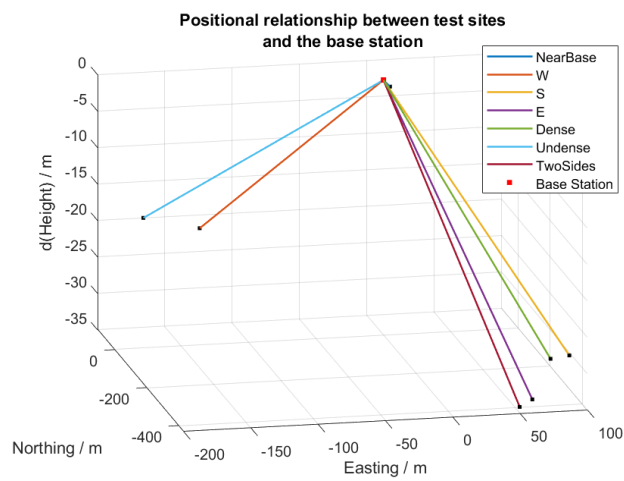


Figure 4.16: 3D positional relationship plot of our sites in Day 2.

beginning of the measurements. According to the test in Day 1, the accuracy of Leica device with NRTK in a clear sky was quite accurate, with an error of 2 cm horizontally and 2.2 cm vertically, therefore it could be used as a precisely known position to set up our u-blox base station.

However, we were not able to measure the position of the top of the billboard directly, because it was hard to hold the long pole of Leica on the top of the billboard. Therefore we had to measure the position of a point on the ground next to the billboard, with a horizontal distance of a few centimeters. This biased position was then set as the precise position of the u-blox base station. We decided to use the Near Base site to compensate this error: its environment was almost the same with the base station, so the error of the Leica device and u-blox would also be similar. We calculated the average position of Leica and u-blox at Near Base respectively and then got the position difference. This difference was used as the bias compensation and is subtracted from measured u-blox data of all other 6 sites. The calculated bias was -0.1402 m in easting direction and 0.049 m in northing.

At each site, instead of putting the GNSS antenna directly on the ground, a triangular metal plate was fixed on the ground and adjusted to horizontal, as Figure 4.17 shows. It was 5-10 cm above the ground. A screw hole on the plate was selected as the exact point to be measured, where the Leica pole was pointed at and the u-blox GNSS antenna was placed on.



Figure 4.17: Measurements were taken on a screw hole of a triangular metal plate.

There were major adjustments to the measuring procedure compared with Day 1. Since the compass on mobile phone we used last time was not so accurate, it might cause large error when the distance of Leica device and u-blox was large. Therefore we decided to measure the exact same point at each site with the two kinds of devices. In order to measure the same point, we were no longer able to collect data from the two devices simultaneously. Instead, we followed the following procedure:

1. Use Leica NRTK to collect at least 25 dots at first.
2. Use u-blox rover to measure the same point and record for at least 15 minutes,

which will become 900 dots. Instead of starting the recording when the first fixed status is reached, we begin to record when the rover is turned on.

3. Use Leica NRTK to collect 25 dots again at the same point. These dot will be combined together with the 25 dots from step 1. Finally, at least 50 dots of Leica NRTK are obtained at each site.

The new procedure also avoided the body of the operator from blocking the satellite signals to u-blox antenna when using Leica device to take measurement close by at the same time.

In addition, since u-blox's RTCM 1230 empty problem was noticed as discussed in Section 2.3.2, this message was turned off in Day 2's measurements. The total number of RTCM sent per second by the base station was then 5.

4.3.3 Test Results Analysis

4.3.3.1 Canopy closure and CNR of satellites

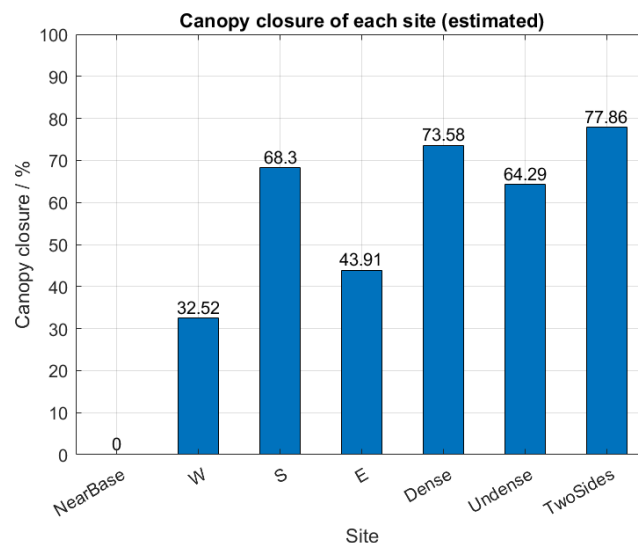


Figure 4.18: Canopy closure percentage of the sites.

The estimated canopy closure of each site is shown in Figure 4.18. Besides the clear sky at Near Base, the sites could be divided into two parts: W and E had an α of 30% ~ 50%; S, Dense, Undense and Two Sides had a worse α of 60% ~ 80%.

The number of satellites observed by u-blox and their CNR at each site is shown in Figure 4.19. It was basically negatively related with the canopy closure. For u-blox, the number of satellites with a CNR above 40 dB (N_{40dB}) was above 10 in every site, therefore no site was in a bad satellite visibility. N_{40dB} was above 20 in sites Near Base, W and E, and was between 10 ~ 20 at the other four sites. Similarly, for Leica, the total number of satellites was still 20~25, with around 20

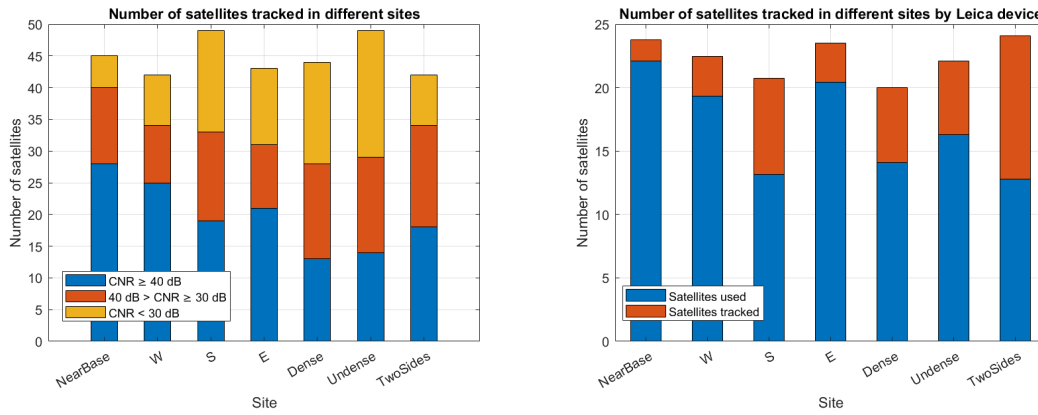


Figure 4.19: Numbers of satellites in different sites tracked by u-blox kit (left) and Leica NRTK (right).

used at Near Base, W and E, while around 15 satellites were used at the other 4 sites.

4.3.3.2 Time to fix and Carrier phase solution

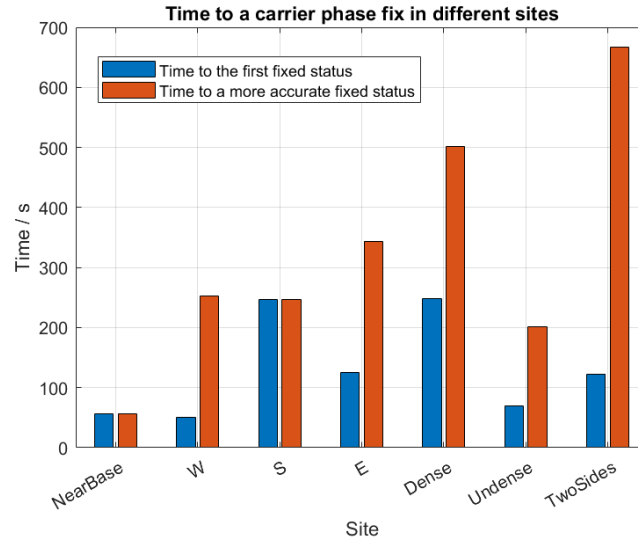


Figure 4.20: Time to fix T_{fix0} and time to a better fix T_{fix} in each site.

The new procedure of measurement made it possible to compare the time to a carrier phase ambiguity fix ever since the device was turned on. The time to the first fix T_{fix0} varied from 50 s at W to 4 min 8 s at Dense.

In this test, the carrier phase status were not always kept fixed in all sites. According to Table 4.4, the rover was in a fixed state for most of the time only at Near Base, W and E (which were also the three sites with low canopy closure). In the other 4 sites, it only reached a fix for a short time, and then lost the fix again. However, cycle slips might happen at any of the sites, regardless it was fixed or not.

In these measurements, the positions from a later fix (or after a cycle slip) were often more accurate than that from the first fix, thus the time to a better fix T_{fix} is introduced. It took more than 3 min for most sites (except Near Base) to achieve a better position. The worst one (Two Sides) spent 11 min 7 s to achieve a more accurate phase ambiguity and a more accurate position.

Only positions after T_{fix} were used later for calculations of standard deviation and positional error.

Table 4.4: Number of points before and after filtering. (Day 2 at Brudareossen)

Site	u-blox			Leica NRTK	
	All	Fixed	Used	All	After filtering
Near Base	902	851	851	60	60
W	997	948	746	56	56 or 30 ¹
S	931	61	712	59	56
E	894	777	557	59	59
Dense	945	93	452	57	57
Undense	951	52	232	52	52
Two Sides	911	47	801	51	51

¹ Only the first 30 dots at W are used to calculate the position, because the triangular plate was moved by mistake before the last 26 dots were collected.

For Leica NRTK device, as listed in Table 4.4, it performed better than those from tests on Day 1, because almost all the dots survived the two filters except for 3 dots at site S whose 3D quality were worse than 0.1 m.

4.3.3.3 Standard deviation and error of position

The comparison of standard deviation σ was shown in Figure 4.21. σ at sites Near Base and E was better than others, while σ at Two Sides was the worst. The σ_{2D} was less than 5 cm in other sites but was 17.15 cm at Two Sides; the σ_H was within 7 cm at other sites but was 11.39 cm at Undense and 58.82 cm at Two Sides.

The σ of Leica NRTK was lower than that of u-blox in all directions at all sites. It was within 1.2 cm in 2D and within 2.5 cm in height. Leica also had the worst σ_H in Two Sides, but the worst σ_{2D} was at site S.

The positional error ΔX , ΔY , ΔZ and the direction of error were compared in Figure 4.22. In these measurements, u-blox and Leica were measuring the exactly same points, so the positional error was the difference between their mean positions. Since the error at Near Base was intentionally set to 0 in order to compensate the base station setting bias, the positional error was only applicable for the other 6 sites.

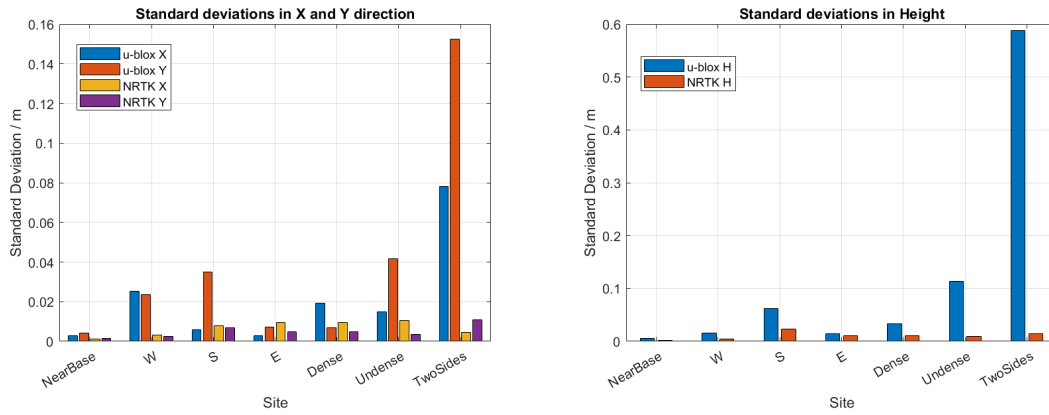


Figure 4.21: Standard deviations of u-blox and Leica NRTK.

Site E had the best result, with a $\Delta 2D$ within 3 cm and a ΔH of 0.3 cm. Errors at sites W and Undense were moderate. They had errors in 2D or H of about 40 cm. Sites S and Dense both had $\Delta 2D$ and ΔH of more than 1 m. There was the worst performance at site Two Sides, with a ΔH of -2.27m and a $\Delta 2D$ of 3.69 m.

From Figure 4.22, it seems that the error in the east-west direction tended to be greater than that in the north-south direction. However, there was not enough data to determine whether the direction of error was related with the direction of the canopy or other factors.

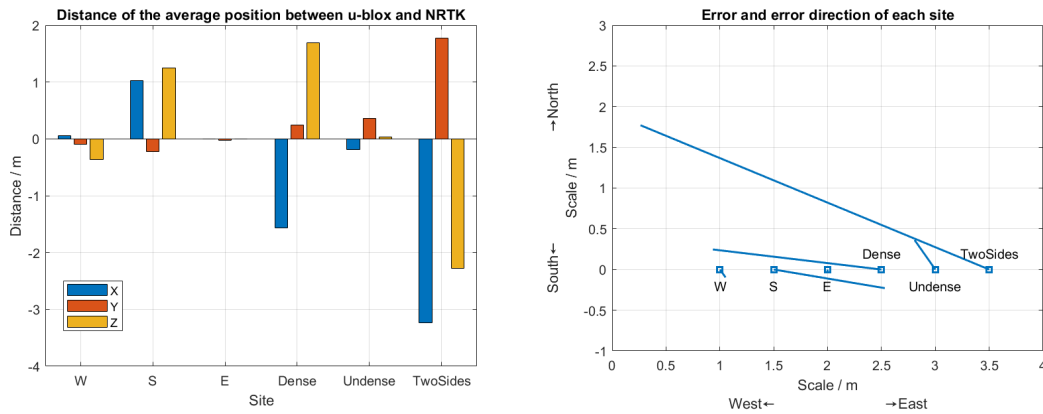


Figure 4.22: Location differences and directions between average locations of u-blox and Leica NRTK. (Directions are all from u-blox to Leica).

4.3.3.4 RTCM and AoD

The average RTCM reception of u-blox at each site is shown in Figure 4.23. In the figure, all the sites had quite good RTCM communication, compared with Day 1. The line-of-sight between base station and site W was interrupted by the terrain, because W was just at the foot of the hill, which was in a convex-shaped terrain. Therefore \overline{N}_{RTCM} at W was only 4.25. All other sites had very smooth RTCM

receptions, with \overline{N}_{RTCM} close to 5.

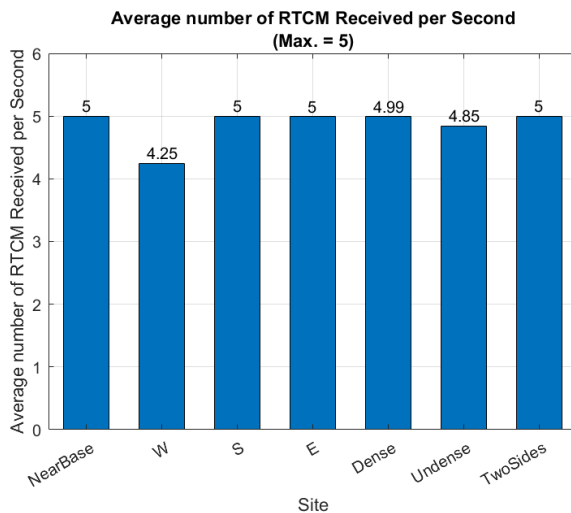


Figure 4.23: \overline{N}_{RTCM} of u-blox at each site in Day 2.

Mean AoD levels and their error bars are shown in Figure 4.24. The age of differential were generally level 1~2 (or within 1~2 s). At some sites, AoD might increase to level 3 (or within 5 s), but only for a short time. Only the maximum of AoD at Site W once reached level 4 (within 10 s).

Since RTCM reception and AoD were mostly ideal for u-blox in Day 2's measurements, they did not contribute much to the error.

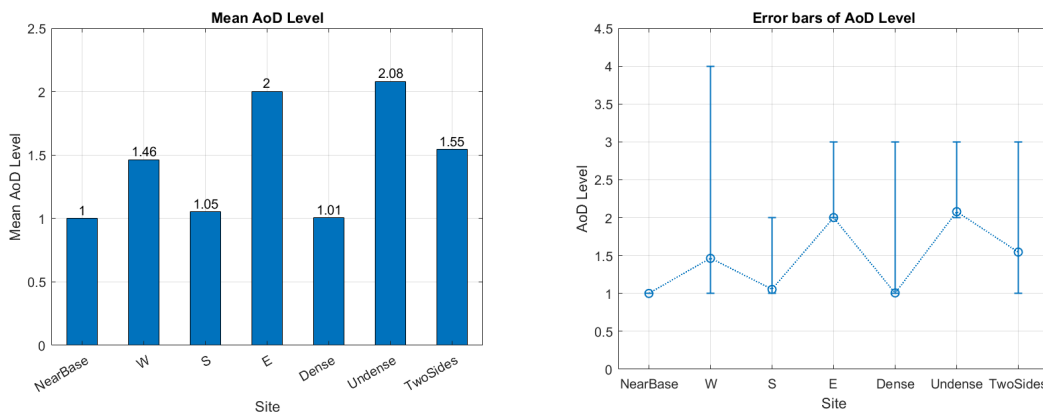


Figure 4.24: Mean AoD level and error bars. For the corresponding relationship between AoD level and time, please refer to Table 3.4.

4.3.3.5 DOP

Horizontal DOP, Vertical DOP and their error bars measured by both devices are shown in Figure 4.25.

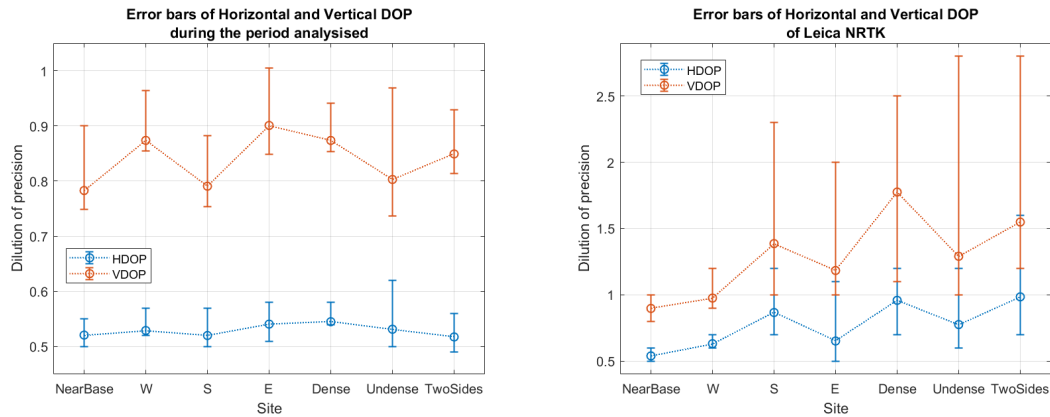


Figure 4.25: Horizontal DOP, Vertical DOP and their error bars measured by u-blox (left) and Leica NRTK (right).

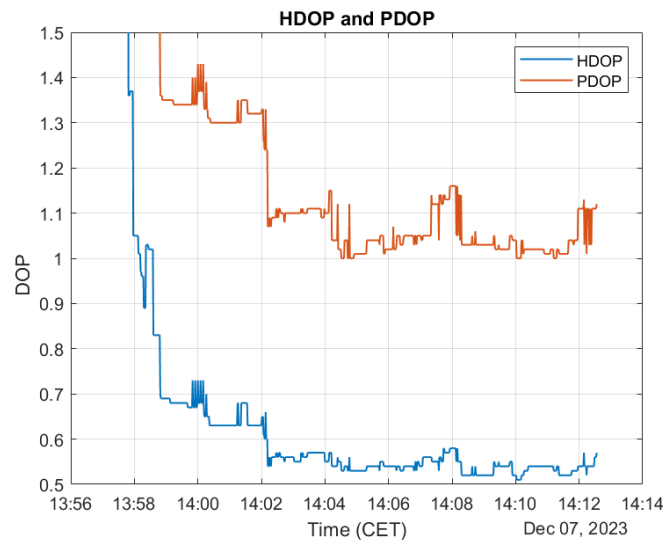


Figure 4.26: The change of DOP with time at site E.

In Day 2's measurements, DOP of u-blox and Leica roughly had negatively relationships with their total numbers of tracked satellites. DOP from Leica showed a similar trend with σ and positional error, but it was not the case for DOP from u-blox. DOP from u-blox seemed to have a similar trend with AoD. However, DOP depends on the distribution and CNR of GNSS satellite, while AoD is related with the quality of RTCM generating and communication. There is no obvious theoretical connection between them, therefore I attribute this relationship to coincidence.

It is found that changes of DOP over time were often reflected in sudden-change events like reaching/losing a fix or suffering from a cycle slip. A good example is shown in Figure 4.26 and 4.27. At site E, u-blox experienced a cycle slip at 14:03:16. In the DOP-time figure, there was an obvious decline for both HDOP and VDOP

4. Measurements and Results

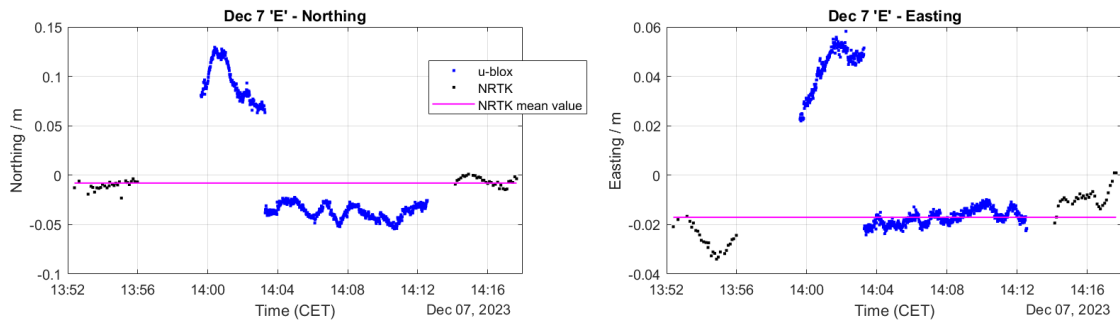


Figure 4.27: Changes of the position of site E over time.

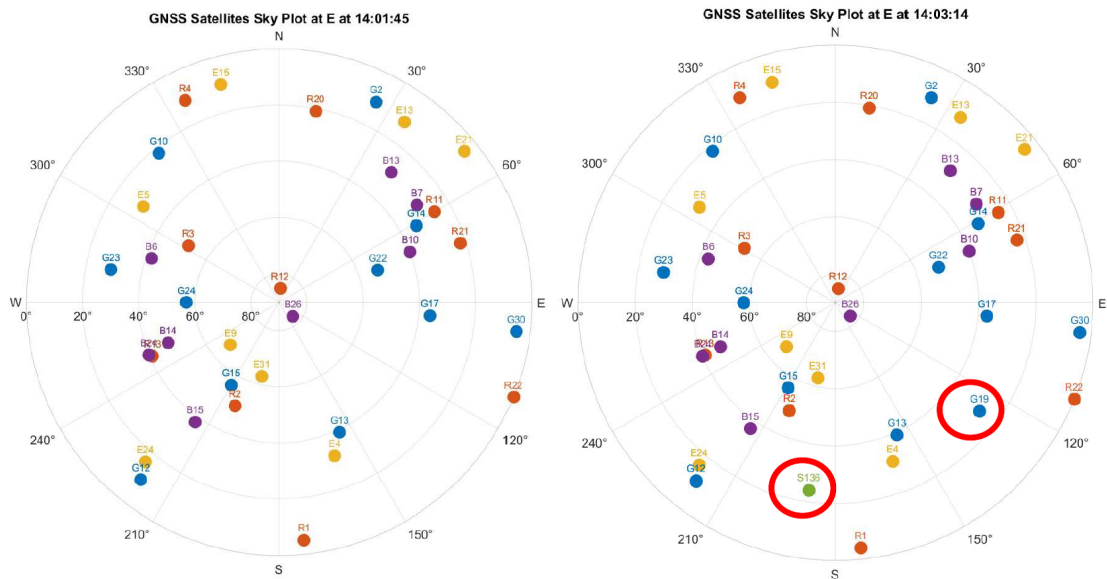


Figure 4.28: Comparison of sky plot before the DOP decline at 14:01:45 (left) and after the DOP decline at 14:03:14 (right) at site E.

about 1 minute before the cycle slip, at around 14:02:10. The PDOP declined from 1.3 to 1.0~1.1.

DOP is highly related to the distribution of GNSS satellites. The sudden change of DOP may indicate that new satellite(s) were starting to be tracked. Comparing the sky plot before and after the decline of DOP, it is found that two new satellites, G19 and S136, were tracked after the decline, as Figure 4.28 shows. These two satellites were in the sky areas that used to be quite empty, thus they had large impacts on DOP. Especially, it is said that the combination of SBAS satellites would improve the DOP by 1.2 to 1.3 times compared with not using SBAS, and the DOP would become more stable [51]. It was verified in this test that the introduction of SBAS improved DOP a lot.

For u-blox, changes of DOP over time before 14 events of reaching a fix or having

a cycle slip during all the measurements in Day 1 and Day 2 were investigated¹. There were obvious signs of DOP declines before 6 of the events, and there were 5 events before which DOP did decline even though it was not obvious. There was over three-quarters probability that a DOP decline could be found within 2 minutes before a sudden-change event occurred.

4.3.4 Analysis Summary

In Day 2's measurements, canopy closure had a greater influence on the error than Day 1. Canopy closure was positively related to positional error at each site. No conclusion could be drawn about whether canopy in the south side had more impact on the measurement than in the east or west side, because the canopy closure of site S was much larger than site E and W. Some areas in low elevations in the north side of the sky were also blocked by the canopy at site S, which was restricted by the test site. Although site S performed worse than W and E, it could not be determined whether the canopy closure or the canopy direction made more contribution. However, the positional error and σ at site S was in a similar level with sites under similar canopy closure but in all directions (Dense and Undense).

Changes of DOP over time had an important impact on the measurement result. A sudden change of DOP would result in cycle slips and/or the achievement or the lost of a fixed state within the coming 1~2 minutes. Since the DOP tended to decline from a large value from the beginning of the test (because the device took time to observe all the satellites gradually), it is therefore recommended to wait for enough time until the DOP becomes more stable before the measured results are put into use. The time to a better fix T_{fix} is a suitable suggestion for this waiting time. It took less than 1 minute for a nice site, about 4 minutes for a medium canopy-level site, and more than 10 minutes for a bad site to achieve a more stable positioning result. However, DOP was not a decisive factor to positional error or σ of the whole measurement. For example, sites W and Two Sides had very similar DOP levels, but the error and σ of Two Sides were obviously worse than W.

RTCM reception was almost ideal and AoD was within 2 s in most cases, therefore they did not contribute much to the error.

In these measurements, the standard deviation σ of Leica NRTK was smaller than that of u-blox in any directions. Dots from NRTK performed very good 3D quality and σ at most of the time. Only at sites W, E and Undense can Leica NRTK be replaced by u-blox, with error of positions $\Delta 2D$ and ΔH less than 40 cm (in which, site E only had an error of 3 cm). At sites S, Dense and Two Sides, the error of positions were over 1 m. Since the error was positively related with canopy closure in Day 2's measurements, it is not recommended to replace u-blox device with Leica NRTK when the canopy closure is larger than 65%.

¹DOP around the following events were investigated: When the first fix was reached at sites W, S, E, Dense, Undense and Two Sides on Day 2; when a later fix or a cycle clip occurred at sites Birch (2), Bank and Oak on Day 1, and at sites W, Dense, Undense and Two Sides on Day 2.

4.4 Correlation Analysis

In order to give suggestions about in which situation can Leica NRTK be replaced by u-blox, it is important to find out the main factors that affect the performance of these devices. Pearson correlation coefficient and Spearman's rank correlation coefficient are therefore introduced, which analyze the linear relationship and the monotonicity between a pair of variables.

In matlab, matrices of variables at each test site are listed, containing σ of u-blox and Leica in all directions, positional error $\Delta 2D$ and ΔH , AoD, DOP, number of satellites N_{sv} , T_{fix0} and T_{fix} measured by u-blox. Environment variables like canopy closure α are also included. We also include the elevation angle from the site to the base station ε_{Base} , trying to abstract the terrain obstacles in the line-of-sight into one variable, because there was roughly convex terrain in our test places. Pearson and Spearman's correlation coefficient of each pair of these variables are calculated.

Table 4.5: Correlation analysis results.

Note: The positive and negative signs in the tables indicate positive or negative correlation. "HH" means very highly, "H" means highly and "M" means moderately correlated. Blank sections represent low relevance or no relevance; "\" represents not applicable.

Day 1	ε_{Base}	σ_{u-blox}	σ_{Leica}	$\Delta 2D$	ΔH	HDOP	VDOP	AoD	α	N_{sv}
σ_{u-blox}	+HH	\	\	+H		+M ^u	+HH ^u			-M ^u
σ_{Leica}	\	\	\		+HH	+H ^L	+HH ^L	\		
$\Delta 2D$	+HH	+H		\	\	+H ^L	\			-H ^u
ΔH			+HH	\	\	\	+H ^L	-M		-M ^u
Day 2	ε_{Base}	σ_{u-blox}	σ_{Leica}	$\Delta 2D$	ΔH	HDOP	VDOP	AoD	α	N_{sv}
σ_{u-blox}		\	\	+H	+M	-M ^u			+M	
σ_{Leica}	\	\	\	+M	+M	+H ^L	+H ^L	\	+HH	-H ^L
$\Delta 2D$		+H	+M	\	\	+H ^L	\		+H	-HH ^L
ΔH		+M	+M	\	\	\	+H ^L		+H	-H ^L
T_{fix}		+H	+M	+H	+H	+H ^L	+H ^L		+H	

^u Only applicable for or have a stronger correlation with data measured by u-blox.

^L Only applicable for or have a stronger correlation with data measured by Leica NRTK.

In Table 4.5, some pairs of parameters that have relatively strong correlations are listed. The measurements in the two days were under quite different condition, therefore they are calculated and listed separately. Due to the uncertainty of the relationship between parameters, the related parameters may not exhibit a linear relationship, but other regular shapes positively or negatively. Therefore, the table is based on the larger value between Pearson's r and Spearman's ρ of each pair of parameters. r or ρ are then replaced with correlation criteria, which was listed in Table 3.3. Parameter pairs with high correlations are also plotted in Figure 4.29 - 4.31.

In the correlation analysis, some conclusions can be made. The conclusions are consistent with the discussions in the previous two sections.

In Day 1's measurement, ε_{Base} was very highly related with σ of u-blox and $\Delta 2D$, which indicates that the convex terrain impacted the performance of u-blox a lot. A larger standard deviation roughly coped with a larger error. DOP played an important role in the performance, and DOP of Leica NRTK had a stronger correlation than that of u-blox. AoD and canopy closure α did not have obvious relationship with σ or positional error, which indicates that they were not the main factor influencing the performance in Day 1's measurement. Number of satellites measured by u-blox had a medium to highly negative relationship with σ or positional error.

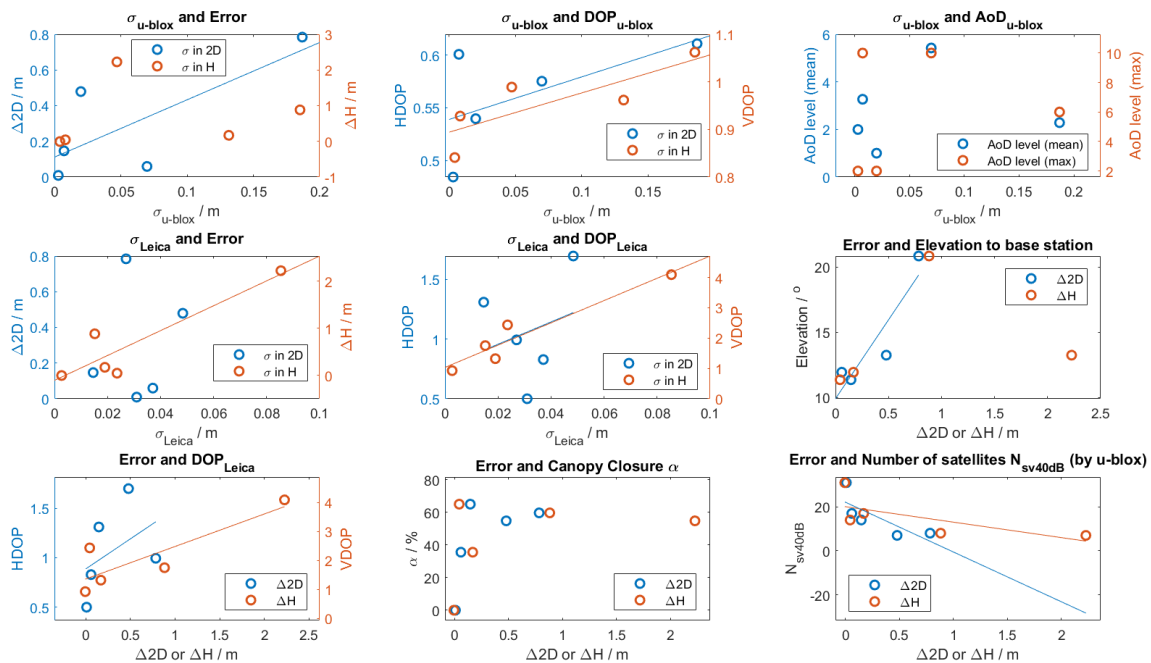


Figure 4.29: Correlation analysis for the test on Day 1.

In Day 2's measurement, the terrain had no obvious impact. A larger standard deviation coped with a larger error. DOP played a less important role in the performance than in Day 1's measurement, while DOP of Leica NRTK was still dominant. AoD was still not related, but the canopy closure α was highly correlated with σ or positional error. Number of satellites measured by Leica had a highly to very highly negative correlation with σ or positional error.

Time to a better fix T_{fix} , as shown in Figure 4.31, was found moderately or highly correlated with σ , positional error, DOP and α in Day 2's measurement.

4. Measurements and Results

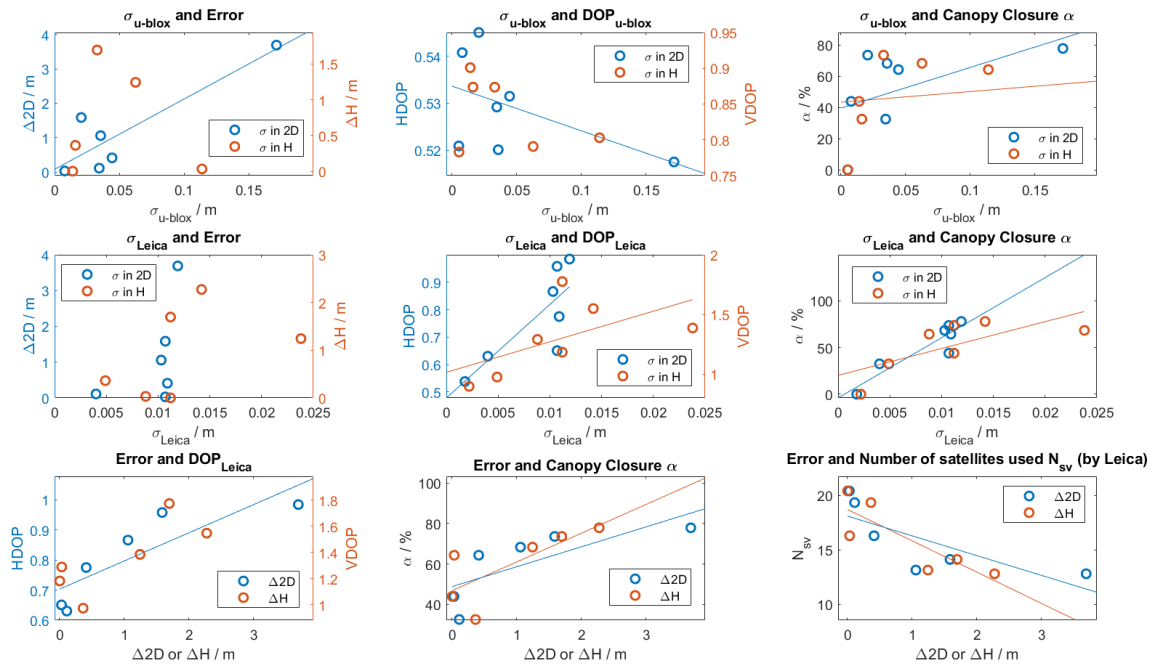


Figure 4.30: Correlation analysis for the test on Day 2.

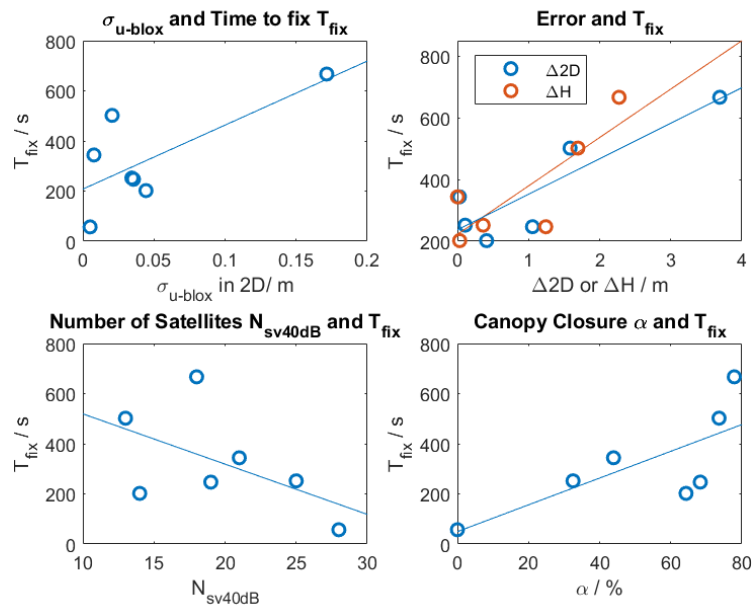


Figure 4.31: Correlations of time to fix T_{fix} and some other variables.

5

Conclusions

5.1 Conclusions

In this project, the u-blox RTK kit we assembled was cheap, lightweight and easy to carry. They are plug-and-play and easier to operate than surveying type receivers. The u-blox device received signals from GPS, GLONASS, Galileo, Beidou, QZSS and EGNOS SBAS and used MSM4 for RTK correction, while Leica was not receiving Beidou signals. We did field measurements at 12 site in two test days. Positional information and other parameters like DOP, AoD and sky plot were collected. The comparisons were made based on positional errors, standard deviations and time to fix.

The canopy closure α was one of the important factor influencing the performance of u-blox and Leica in the forest. The project is just a case study and the two measurement days were quite different in location, weather and time of year, therefore the importance of α also varied. If the positional error is required to be less than 50 cm, the recommended maximum α turned out to be about 50% for Day 1 and 65% for Day 2. In our measurements, all the sites that fulfilled this requirement were only half-covered by the canopy or had a clear sky. Only one test site that covered by the canopy in all directions (site Undense, Day 2, with $\alpha = 64.29\%$) had an positional difference of less than 50 cm between the results of u-blox and Leica. When α was below 45%, the positional error had a possibility to reach centimeter level (site E on Day 2, site Bank on Day 1 and Near Base on both days), but may also be still a few decimeters (site W on Day 2). The requirement for α reveals that the u-blox kit is not capable to replace the surveying type Leica NRTK in many situations with dense forests.

DOP was the other important factor for both days' measurements. DOP had medium to very highly positive relationship with the standard deviations or positional error. The DOP in Day 1 was overall worse than that of Day 2, thus the canopy limit of Day 1 was also lower. For the u-blox device, DOP values were usually high and fluctuating in the beginning, but they became lower and more stable when more satellites were tracked, thus it is recommended to wait for a while after turning on the device. The waiting time until a better fix could be 4 min in medium canopy-level forests or more than 11 min in dense forests. From Day 1's result, it is generally recommended to avoid an HDOP above 0.60 or a VDOP over 0.95. For Leica device, the 3D quality of a large percentage of collected positions tended to

be bad (> 0.1 m) when HDOP was above 1.3 and VDOP was above 2.0.

There was no obvious pattern in the direction of positional error. No connection between the direction of error and the direction of canopy could be found. However, the standard deviation in height σ_H was usually larger than σ_X or σ_Y . This is reasonable, because VDOP is generally larger than HDOP due to the distribution of satellites, therefore the uncertainty is larger in the vertical direction. For u-blox, σ became significantly large when the carrier phase fix was not achieved or cycle slips happened. In good conditions, σ was 3 cm in X or Y direction and 5 cm in height, but it increased to a few decimeters when α or DOP became worse. The standard deviations of Leica in all directions could reach sub-centimeter level and were usually less than 2 cm, except for site Birch (2) on Day 1, with a σ_H of 8 cm. In 10 of our 12 sites, σ_{Leica} was smaller than σ_{u-blox} in all directions, despite the DOP values were worse for Leica.

The RTCM reception and the AoD of correction messages had no obvious relationship with positional error or standard deviation for u-blox. However, it does not mean that we do not need to care about it. A too long AoD usually means the RTCM has been interrupted for a long time. The u-blox device was able to achieve a carrier phase fix only when correction messages are received. The maximum of AoD was no more than level 2 (age < 2 s) for all of the sites. Sometimes the fix state could still be maintained when level 5 (age < 15 s) was reached for a while (site Oak, Day 1), but a long break of RTCM was very likely to result in a lost of fix.

According to the pretests, the RTCM reception is sensitive to the terrain obstacles in the line-of-sight between the base station and the rover. According to Fresnel zone theory, it is recommended to mount the RTCM radio antennas at a higher place to extend the range. It would be the best to have an unobstructed line-of-sight between the base station and the site of interest. A confidence RTCM communication range in our measurements is 500 m. This is also one of the difficulties for u-blox to replace Leica NRTK, because NRTK normally does not have this limit. However, it is worth pointing out that RTCM is not a feature of u-blox itself, and a better RTCM communication would enable the equipment to perform at its best. Meanwhile for NRTK, the RTCM can be retrieved once it is connected to SWEPOS through the Internet. The AoD for SWEPOS is always less than 3 s, which is an ideal value.

On Day 2 a comparison between different canopy directions (W, S, E, Two Sides) were made. The sky plots in Appendix B did not show obvious different distributions when canopy directions were different. The positional error and standard deviation of site S was much larger than sites W and E, while those of Two Sides was much larger than S. Although the canopy closure α of site S was larger than W and E, because canopy also existed at low elevations in the north side at site S, but a major area of high elevations in the north side was still empty, so that it was supposed not to affect the performance very much. However, their errors were also strongly monotonically related to α . It showed that blocking south side or two sides of the sky had some influence to the performance, but the canopy closure had a greater impact.

No conclusions could be made about whether the species of trees affected the performance, because there were not enough data. Birches, oaks, pines and firs were involved in the measurements, but they were not controlled variables, for other conditions (e.g. canopy closure α , direction and density of trees) varied a lot. However, since trees and their leaves only acted as obstacles in the way of signal propagation, the difference of species could also correspond to different canopy closure, therefore the question becomes which species had higher canopy closures. For the canopy closures in Figures 4.3 and 4.18, it is found that sites with oaks and firs were likely to have larger α than sites with birches and pines, and thus performed worse. However, it was only based on a few sites and rough estimations of α , so it is worthwhile to do further studies on this topic.

5.2 Future works

The project is only a case study in specific locations and environments in November and December with very limited data. Further studies can be repeated in different seasons, weathers and locations to obtain a more comprehensive view on the result. It is also worth taking measurements for a longer time to collect more data and to analyze its long-term performance and stability.

Due to the time limit, we only analyzed the performance of low-cost traditional RTK and professional network RTK in some of the aspects. There are still some aspects worthy of analysis in the future.

It is a problem that the applicable distance of RTCM is shorter than claimed on the fact sheet of the LR antenna in the u-blox kit. On one hand it is needed to have a more detailed analysis on how far away and in which kind of terrain will the RTCM signal be blocked. On the other hand, we should find out a way to extend this range or replace it with a better antenna.

The estimation of canopy closure in this work is only a rough method and can be improved. Especially, it is recommended to use a fish-eye lens to take the photos, and to give larger weights to the canopy at higher elevations, in order to be more suitable for applying to GNSS, because the GNSS signals at high elevations are usually in a better CNR and play more important roles.

For low-cost RTK devices, we are only able to test the u-blox F9P device due to time limit, but other different low-cost devices may also be worth comparing. For network RTK, as introduced in Section 2.3.3, SWEPOS is going to start supporting Beidou satellites in the near future. It can be expected that the performance of professional network RTK would be even better. There may be a different comparison result when Beidou comes into use in SWEPOS.

Bibliography

- [1] Atınc Pırtı et al. “An alternative method for point positioning in the forested areas”. In: *Šumarski List* 140 (2016), pp. 155–163.
- [2] Feng Tong et al. “Effects of Canopy and Multi-Epoch Observations on Single-Point Positioning Errors of a GNSS in Coniferous and Broadleaved Forests”. In: *Remote Sensing* 13.12 (2021), p. 2325.
- [3] Atınc Pırtı and M. Ali Yucel. “Evaluating Repeatability of RTK (GPS and Galileo/GPS) performance in the analysis of points located in areas with and without obstructions”. In: *Reports on Geodesy and Geoinformatics* 113.1 (2022), pp. 11–20.
- [4] Andreas, Heri et al. “Study the capabilities of RTK Multi GNSS under forest canopy in regions of Indonesia”. In: *E3S Web Conf.* 94 (2019), p. 01021.
- [5] Omid Abdi et al. “Evaluation of Forest Features Determining GNSS Positioning Accuracy of a Novel Low-Cost, Mobile RTK System Using LiDAR and TreeNet”. In: *Remote Sensing* 14.12 (2022), p. 2856.
- [6] Pete Bettinger and SongLin Fei. “One Year’s Experience with a Recreation-Grade GPS Receiver”. In: *Mathematical and Computational Forestry & Natural Resource Sciences* 2.2 (Aug. 2010), pp. 153–160.
- [7] Tomoji Takasu. *Diary/Memorandum*. in Japanese. Research and Development of Precise Positioning Technology by Global Navigation Satellite System. <https://gpspp.sakura.ne.jp/diary202107.htm>. July 2021.
- [8] Thomas Purfürst. “Evaluation of Static Autonomous GNSS Positioning Accuracy Using Single-, Dual-, and Tri-Frequency Smartphones in Forest Canopy Environments”. In: *Sensors* 22.3 (2022), p. 1289.
- [9] Ramazan Akbulut et al. “Effects of forest thinning on static horizontal positions collected with a mapping-grade GNSS receiver”. In: *Mathematical and Computational Forestry & Natural Resource Sciences* 9.1 (2017), pp. 14–21.
- [10] Atınc Pırtı and Ramazan Gürsel Hoşbaşı. “Evaluation of the performance between post process kinematic and static technique in the forest environment”. In: *Šumarski List* 145 (7-8) (2016), pp. 367–376.
- [11] Michał Brach. “Rapid Static Positioning Using a Four System GNSS Receivers in the Forest Environment”. In: *Forests* 13.1 (2022), p. 45.
- [12] Steven A. Weaver et al. “How a GNSS Receiver Is Held May Affect Static Horizontal Position Accuracy”. In: *PLoS One* 10.4 (Apr. 2015).
- [13] United States Coast Guard. *Global Positioning System (GPS) Overview*. Navigation Center. <https://www.navcen.uscg.gov/global-positioning-system-overview> (Accessed 1 Feb. 2024).

- [14] Bart Hendrickx. *The secret payloads of Russia's Glonass navigation satellites*. The Space Review. <https://www.thespacereview.com/article/4502/1>. Dec. 2022.
- [15] The European Space Agency. *Galileo satellites*. https://www.esa.int/Applications/Navigation/Galileo/Galileo_satellites (Accessed 1 Jan. 2024).
- [16] China Satellite Navigation Office. *BeiDou Navigation Satellite System Open Service Performance Standard (Version 3.0)*. May 2021.
- [17] National Space Policy Secretariat. *Advantages of QZSS*. Quasi-Zenith Satellite System (QZSS). <https://qzss.go.jp/en/overview/services/superiority.html> (Accessed 1 Jan. 2024).
- [18] Wei Xie et al. "Characteristics and Performance Evaluation of QZSS Onboard Satellite Clocks". In: *Sensors* 19.23 (2019), p. 5147.
- [19] ESA Navipedia. *EGNOS General Introduction*. https://gssc.esa.int/navipedia/index.php?title=EGNOS_General_Introduction (Accessed 1 Jan. 2024).
- [20] Leica Geosystems. *Leica GS18 I Data sheet*. <https://leica-geosystems.com/en-us/products/gnss-systems/smart-antennas/leica-gs18i>. 2022.
- [21] Sergey Karutin. *GLONASS: The decade of transition to CDMA signals*. GPS World. <https://www.gpsworld.com/glonass-the-decade-of-transition-to-cdma-signals/>. Dec. 2023.
- [22] *GPS Errors and Biases Part 2*. what-when-how In Depth Tutorials and Information. <https://what-when-how.com/gps/gps-errors-and-biases-part-2/> (Accessed 1 Jan. 2024).
- [23] Geoffrey Blewitt. "Basics of the GPS Technique: Observation Equations". In: *Geodetic Applications of GPS*. 1997.
- [24] P. Cheng. "Remarks on Doppler-aided smoothing of code ranges". In: *Journal of Geodesy* 73 (Feb. 1999), pp. 23–28.
- [25] Z. Zhou and B. Li. "Optimal Doppler-aided smoothing strategy for GNSS navigation". In: *GPS Solutions* 21 (Jan. 2017), pp. 197–210.
- [26] Brian Bramanto et al. *Long-range Single Baseline RTK GNSS Positioning for Land Cadastral Survey Mapping*. 2019.
- [27] u-blox. *u-blox F9 HPG 1.32: u-blox F9 high precision GNSS receiver Interface Description*. https://content.u-blox.com/sites/default/files/documents/u-blox-F9-HPG-1.32_InterfaceDescription_UBX-22008968.pdf. Mar. 2022.
- [28] Sleewaegen, Jean-Marie et al. "Demystifying GLONASS Inter-Frequency Carrier Phase Biases". In: *Inside GNSS* (May 2012), pp. 57–61.
- [29] u-blox Support Community. *RTCM 1230 empty. Episode II*. <https://portal.u-blox.com/s/question/0D52p00009HIVuWCAT/rtcm-1230-empty-episode-ii>. Sept. 2020.
- [30] Sleewaegen, J-M. et al. "Origin and Compensation of GLONASS Inter-frequency Carrier Phase Biases in GNSS Receivers". In: *Proceedings of the 25th International Technical Meeting of the Satellite Division of The Institute of Navigation (ION GNSS 2012)*. Nashville, TN, Sept. 2012, pp. 2995–3001.

-
- [31] Lantmäteriet. *Kartstöd*. in Swedish. <https://swepos.lantmateriet.se/services/mapservice.aspx> (Accessed 1 Jan. 2024).
- [32] Lantmäteriet. *Testa satellitsystemet Beidou i Swepos Nätverks-RTK*. in Swedish. <https://www.lantmateriet.se/sv/geodata/gps-geodesi-och-swepos/swepos/testa-satellitsystemet-beidou-i-swepos-natverks-rtk/> (Accessed 1 Jan. 2024).
- [33] LESOL Aviation. *WGS – 84 Survey*. <https://www.lesoloaviation.com/WGS%20%E2%80%93%2084%20Survey.html> (Accessed 1 Jan. 2024).
- [34] Intergovernmental Committee on Surveying and Mapping. *Datums Explained in More Detail*. Fundamentals of Mapping - Datums. <https://www.icsm.gov.au/education/fundamentals-mapping-datums/datums-explained-more-detail> (Accessed 5 Jan. 2024).
- [35] Lantmäteriet. *Transformation between ITRF 2014/WGS 84 and SWEREF 99*. <https://www.lantmateriet.se/sv/geodata/gps-geodesi-och-swepos/Transformationer/ITRF---SWEREF-99>. June 2023.
- [36] Lantmäteriet. *Simple coordinate transformation*. <https://www.lantmateriet.se/en/geodata/gps-geodesi-och-swepos/geodesy/geodesy-services/simple-coordinate-transformation/> (Accessed 1 Mar. 2024).
- [37] Robert Larsson. *RT90, WGS84 och SWEREF99*. in Swedish. <https://rl.se/rt90> (Accessed 1 Jan. 2024).
- [38] Fredrik. *WGS 84 to SWEREF*. MATLAB Central File Exchange. <https://www.mathworks.com/matlabcentral/fileexchange/36945-wgs-84-to-sweref>. 2012.
- [39] Lantmäteriet. *Compute geoid height*. <https://www.lantmateriet.se/en/geodata/gps-geodesi-och-swepos/geodesy/geodesy-services/compute-geoid-height/> (Accessed 1 Jan. 2024).
- [40] ArduSimple. *simpleRTK2B – Starter Kit LR*. <https://www.ardusimple.com/product/simplertk2b-starter-kit-lr-ip65/> (Accessed 1 Jan. 2024).
- [41] SparkFun Electronics. *SparkFun OpenLog - DEV-13712*. Product Categories. <https://www.sparkfun.com/products/13712> (Accessed 1 Jan. 2024).
- [42] Trimble. *NMEA-0183 messages: Overview*. Alloy Receiver Help. https://receiverhelp.trimble.com/alloy-gnss/en-us/NMEA-0183messages_MessageOverview.html (Accessed 1 Jan. 2024).
- [43] SEMU Consulting. *Python library for reading, parsing and generating NMEA, UBX and RTCM3 GNSS messages*. GitHub repository. <https://github.com/semuconsulting/pygnssutils>. 2022.
- [44] Lauri Korhonen et al. “Estimation of forest canopy cover: A comparison of field measurement techniques”. In: *Silva Fennica* 40 (2006), pp. 577–588.
- [45] SB Jennings, ND Brown, and D Sheil. “Assessing forest canopies and understorey illumination: canopy closure, canopy cover and other measures”. In: *Forestry: An International Journal of Forest Research* 72.1 (Mar. 1999), pp. 59–74. ISSN: 0015-752X.
- [46] Ruiguang Wang et al. “Performance of Smartphone BDS-3/GPS/Galileo Multi-Frequency Ionosphere-Free Precise Code Positioning”. In: *Remote Sensing* 15.22 (2023). ISSN: 2072-4292.

- [47] Oguz Kagan Isik et al. “Integrity Analysis for GPS-Based Navigation of UAVs in Urban Environment”. In: *Robotics* 9.3 (2020). ISSN: 2218-6581.
- [48] J. Fowler, L. Cohen, and P. Jarvis. *Practical Statistics for Field Biology*. Artech House mobile communications series. John Wiley & Sons, 2009, p. 132. ISBN: 9780471982968.
- [49] Yijian Cui et al. “Feasibility analysis of low-cost GNSS receivers for achieving required positioning performance in CAV applications”. In: *2017 Forum on Cooperative Positioning and Service (CPGPS)*. 2017, pp. 355–361.
- [50] James; Ransom Michael D.; Rhynold and Pete Bettinger. “Performance of Mapping-Grade GPS Receivers in Southeastern Forest Conditions”. In: *RURALS: Review of Undergraduate Research in Agricultural and Life Sciences* 5.2 (Aug. 2010). Iss. 1 , Article 2.
- [51] Huu Cong Do and Nguyen Ngoc Lau. “Research on the combination of GPS and SBAS satellites in point positioning”. In: *International Symposium on Geo-spatial and Mobile Mapping Technology and Summer School for Mobile Mapping Technology (GMMT 2016)*. Jan. 2016, Commission VI, WG VI/4.

A

Figures of measured positions varying with time at each site

This appendix shows figures of easting, northing, 2D position and height changing over time in each of our sites. For u-blox, data in unstable time periods are not displayed. Only data from the periods that are stable enough to calculate the positional error and the standard deviation are shown. Typically, they occurred when there was a carrier phase fix (if applicable). For Leica NRTK, only dots that passed the filters in Table 4.2 are shown.

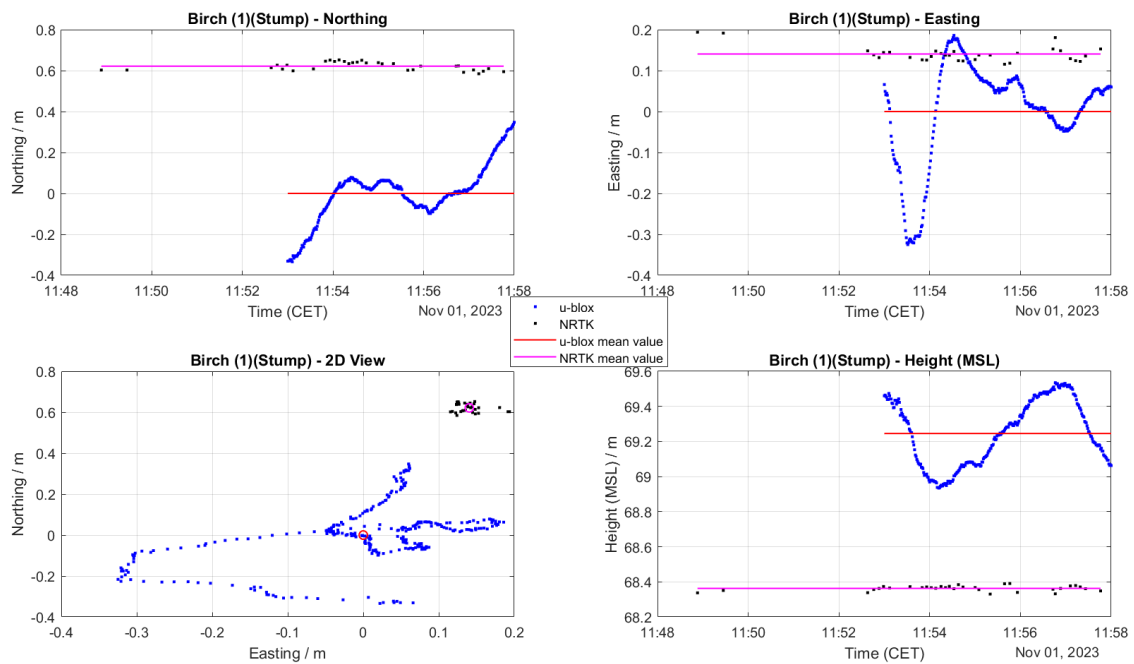


Figure A.1: Site Birch (1), Day 1.

A. Figures of measured positions varying with time at each site

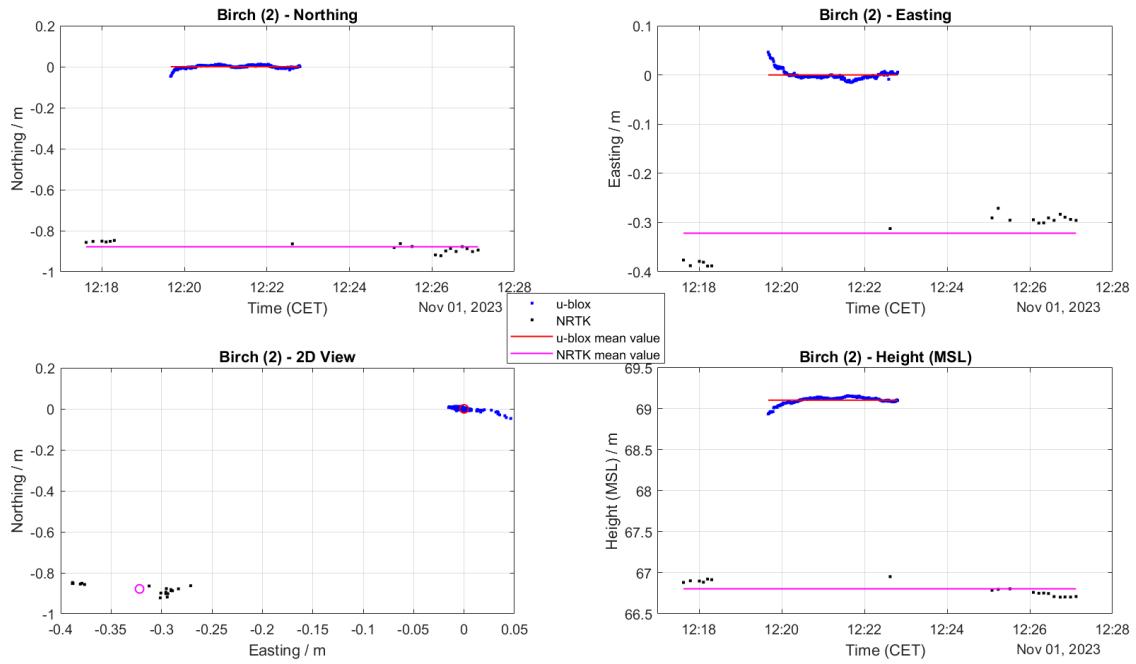


Figure A.2: Site Birch (2), Day 1.

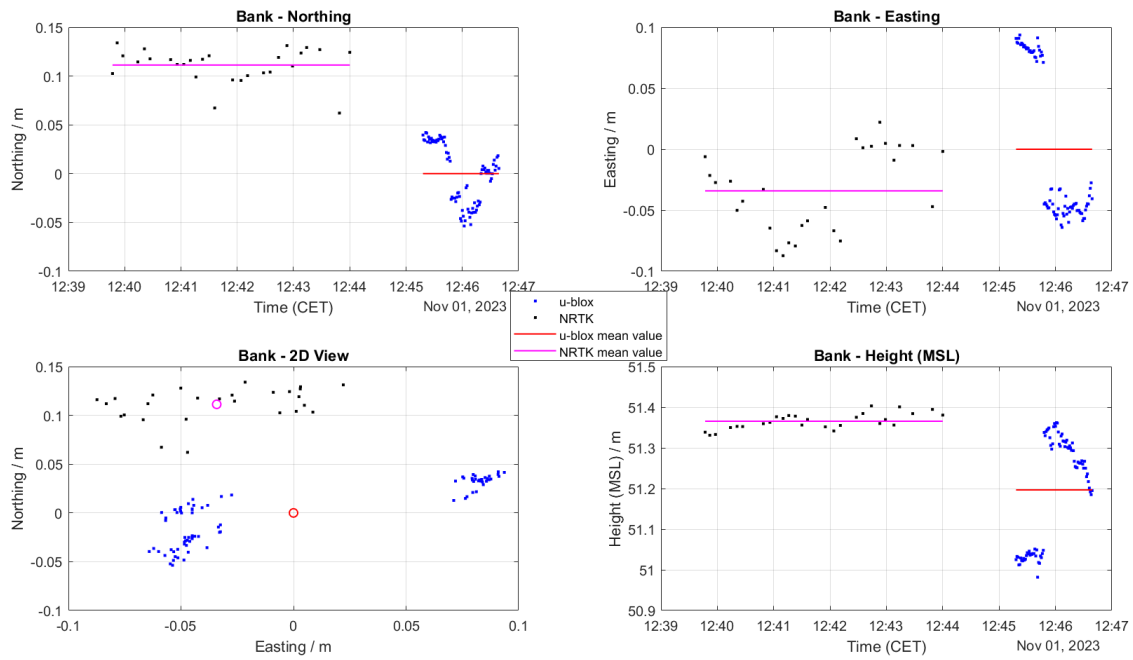


Figure A.3: Site Bank, Day 1.

A. Figures of measured positions varying with time at each site

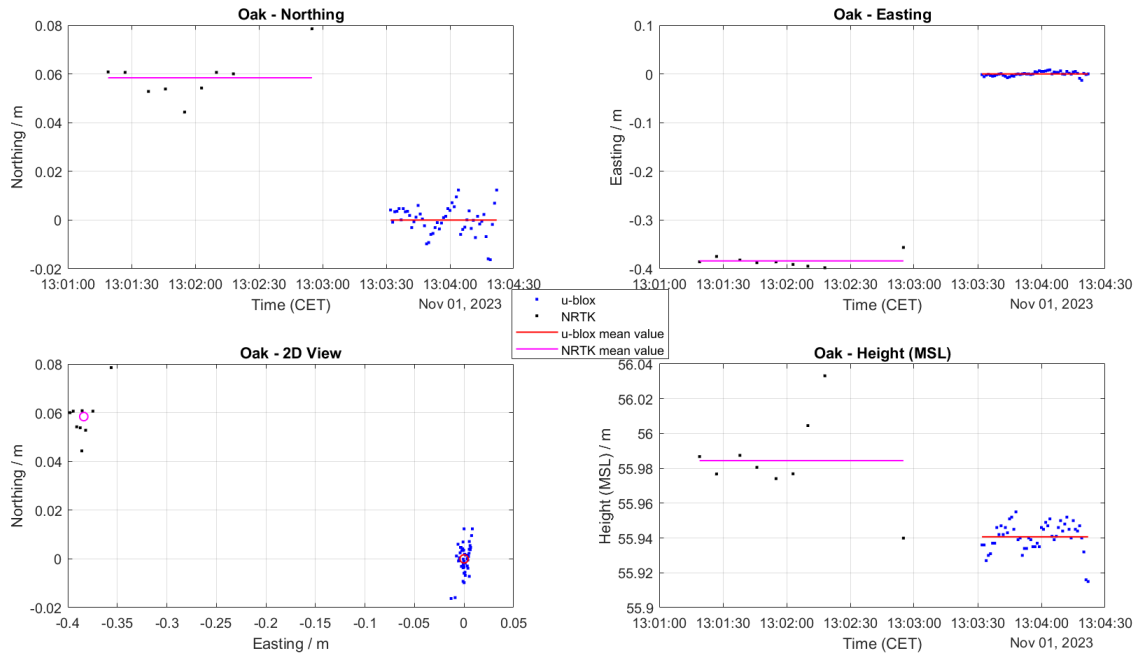


Figure A.4: Site Oak, Day 1.

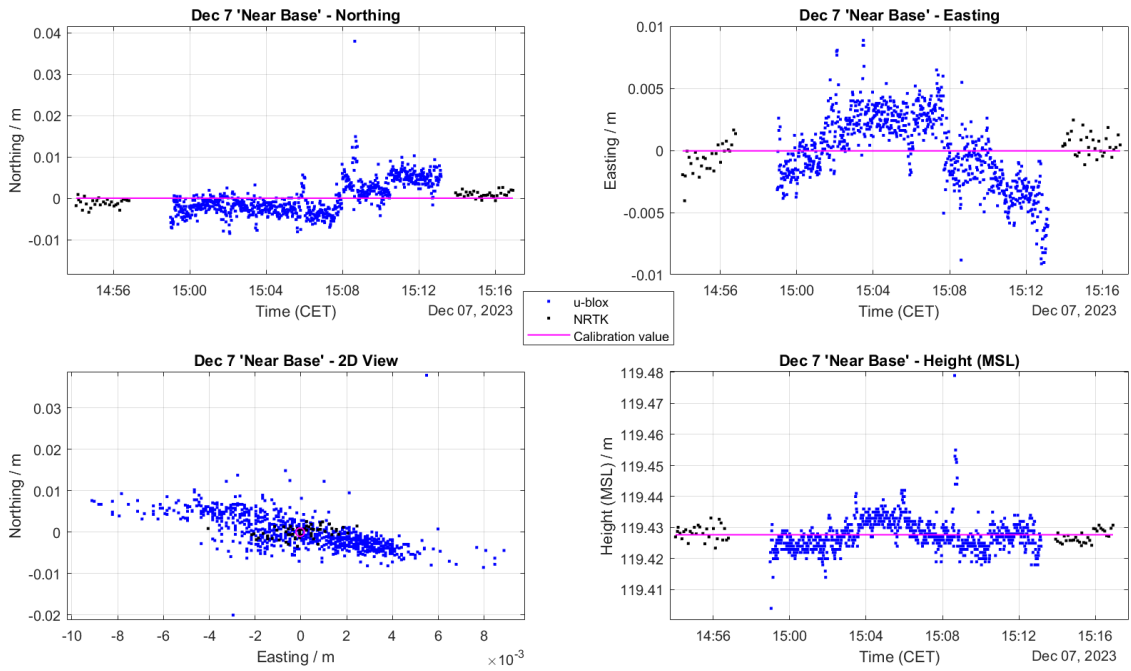


Figure A.5: Site Near Base, Day 2.

A. Figures of measured positions varying with time at each site

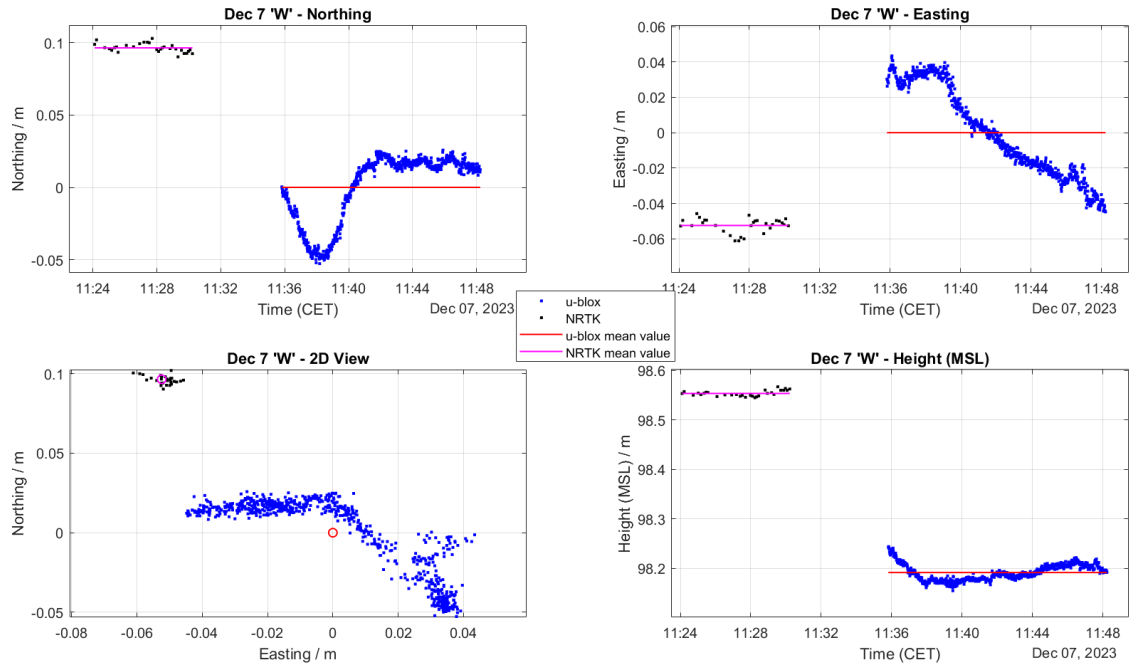


Figure A.6: Site W, Day 2.

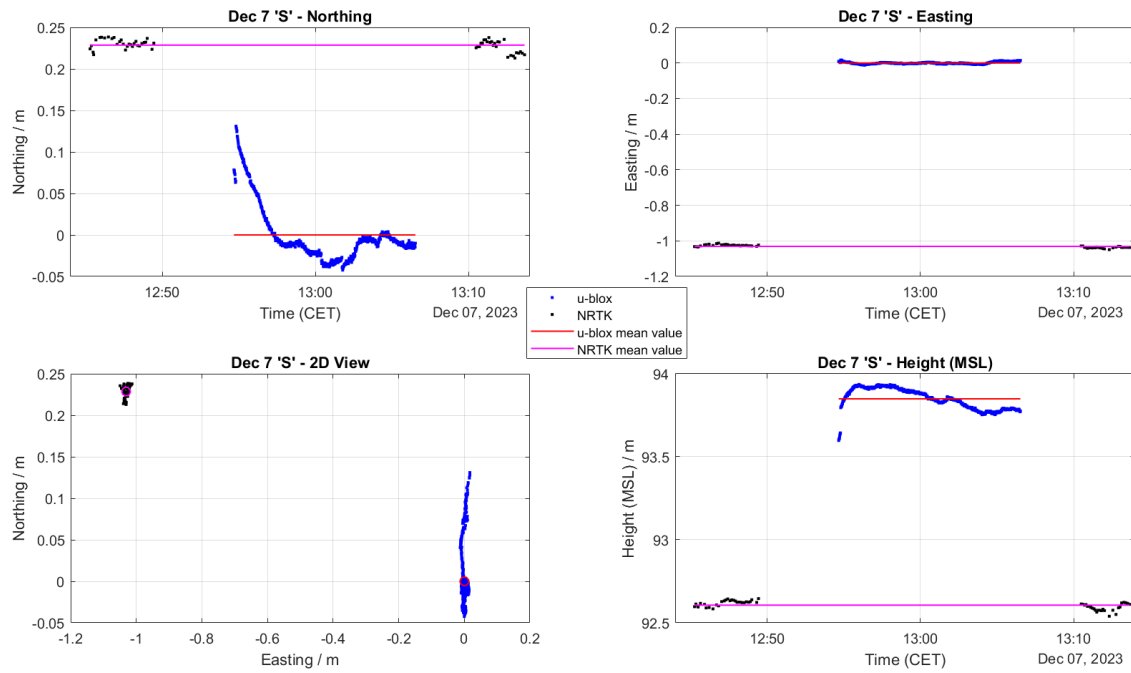


Figure A.7: Site S, Day 2.

A. Figures of measured positions varying with time at each site

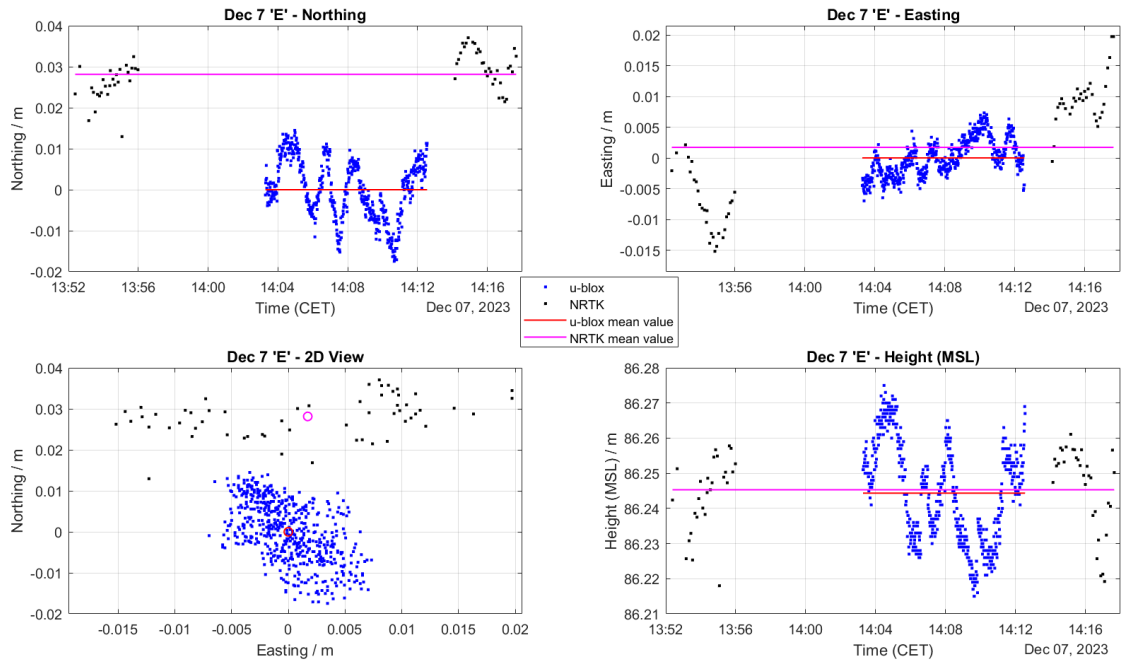


Figure A.8: Site E, Day 2.

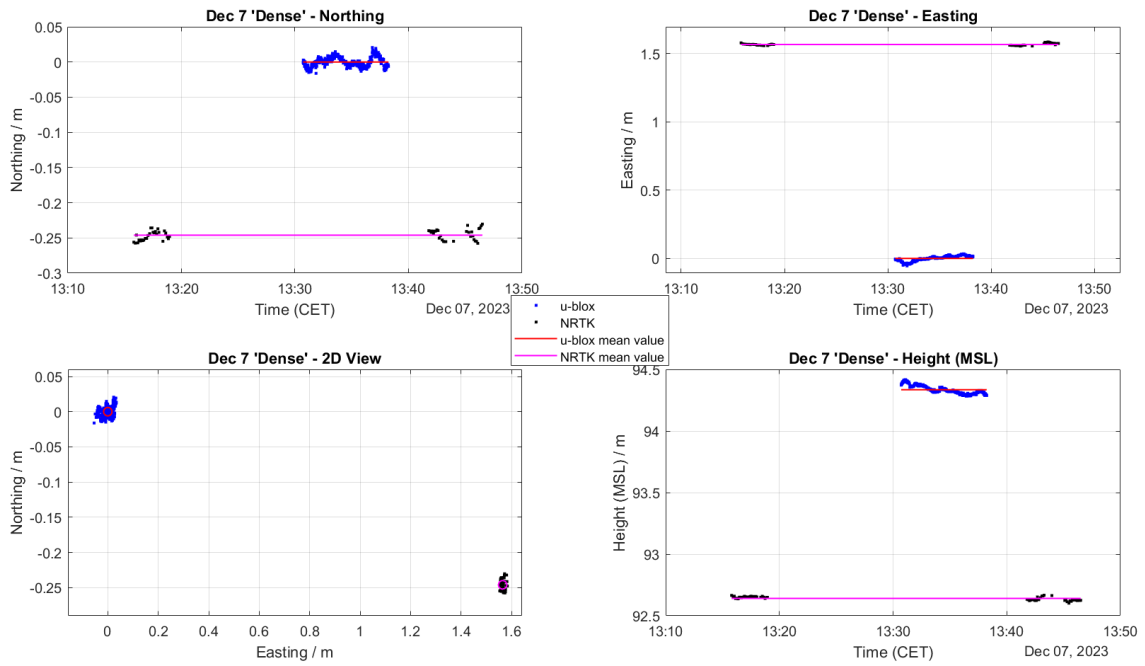


Figure A.9: Site Dense, Day 2.

A. Figures of measured positions varying with time at each site

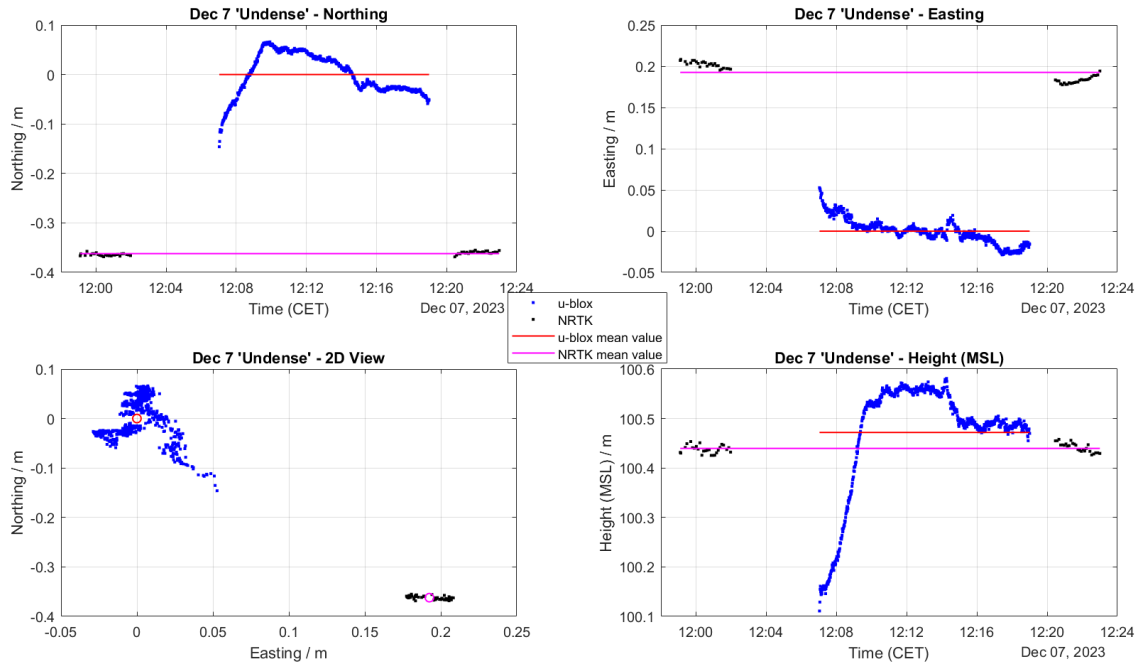


Figure A.10: Site Undense, Day 2.

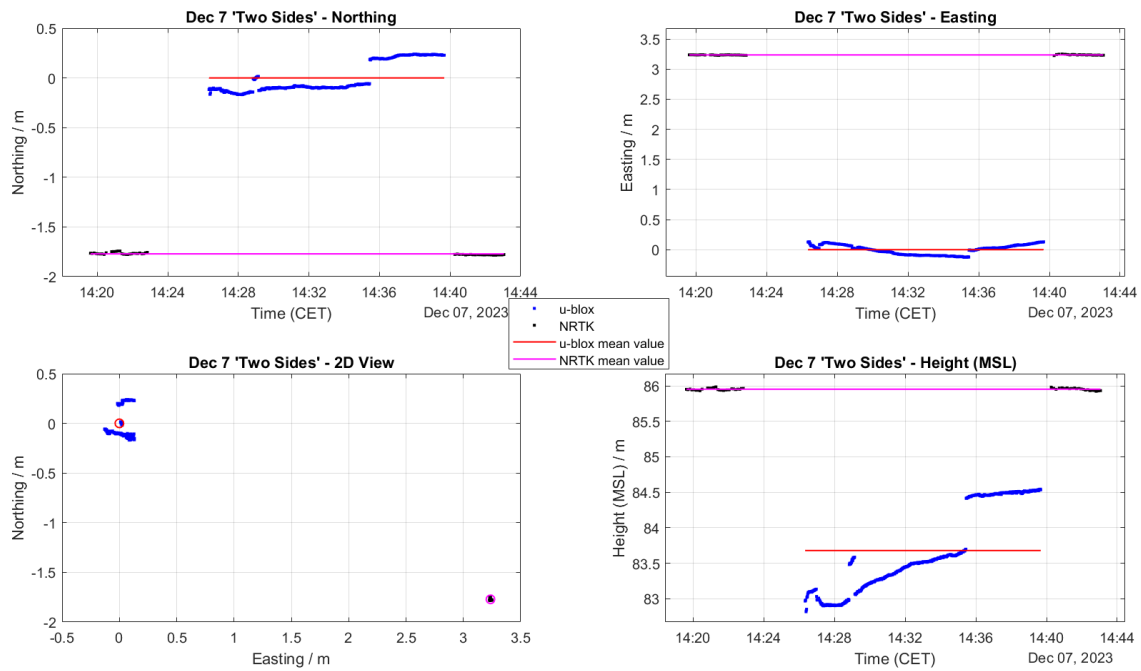


Figure A.11: Site Two Sides, Day 2.

B

Sky plot of GNSS satellites at each site

This appendix shows sky plots of GNSS satellites at each site. The sky plots were taken at a moment when the best fix of the measurements was achieved and the measured position was stable (if possible). Only satellites with a CNR of better than 30 dB are shown in the plots. Different color represents satellites from different GNSS systems. The sky plots are derived from NMEA GNGSV messages and satellite IDs are recognized according to Table 2.2.

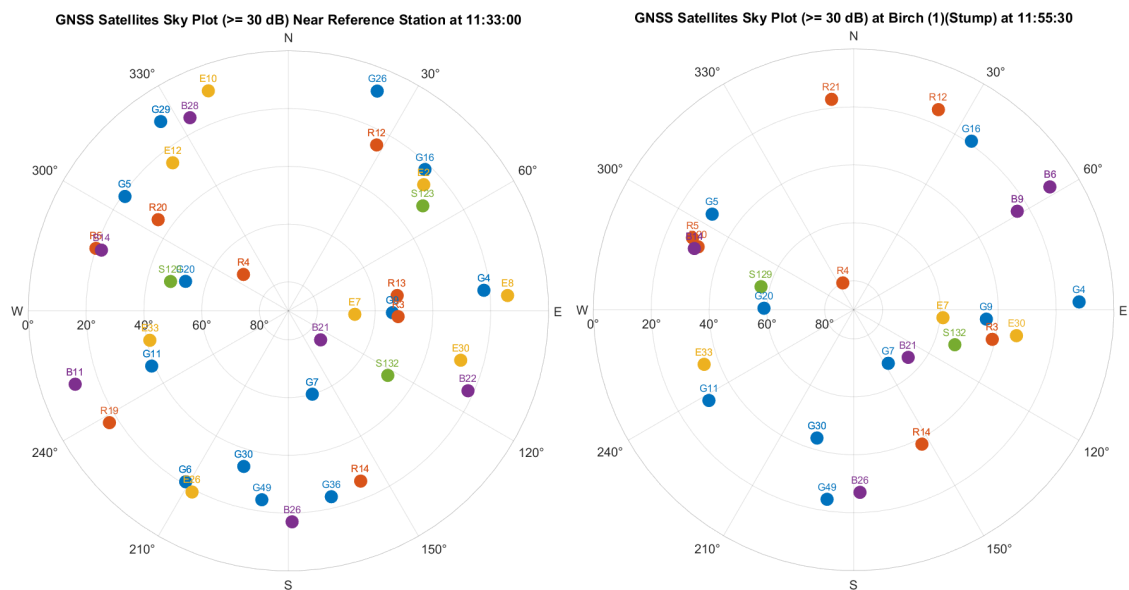


Figure B.1: Site Near Base, Day 1 (left); Site Birch (1), Day 1 (right).

B. Sky plot of GNSS satellites at each site

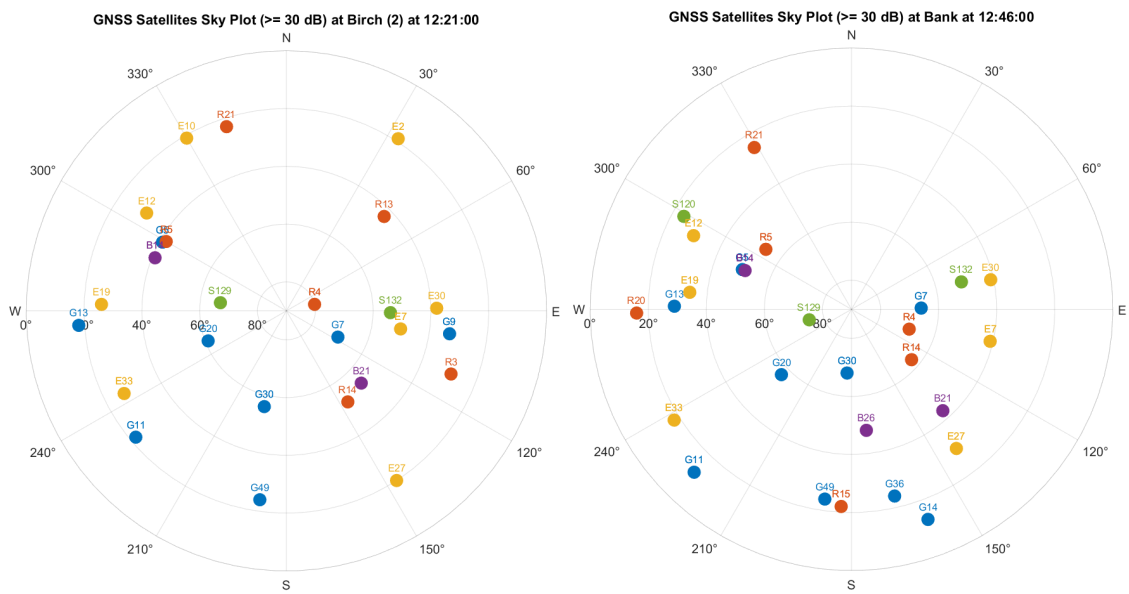


Figure B.2: Site Birch (2), Day 1 (left); Site Bank, Day 1 (right).

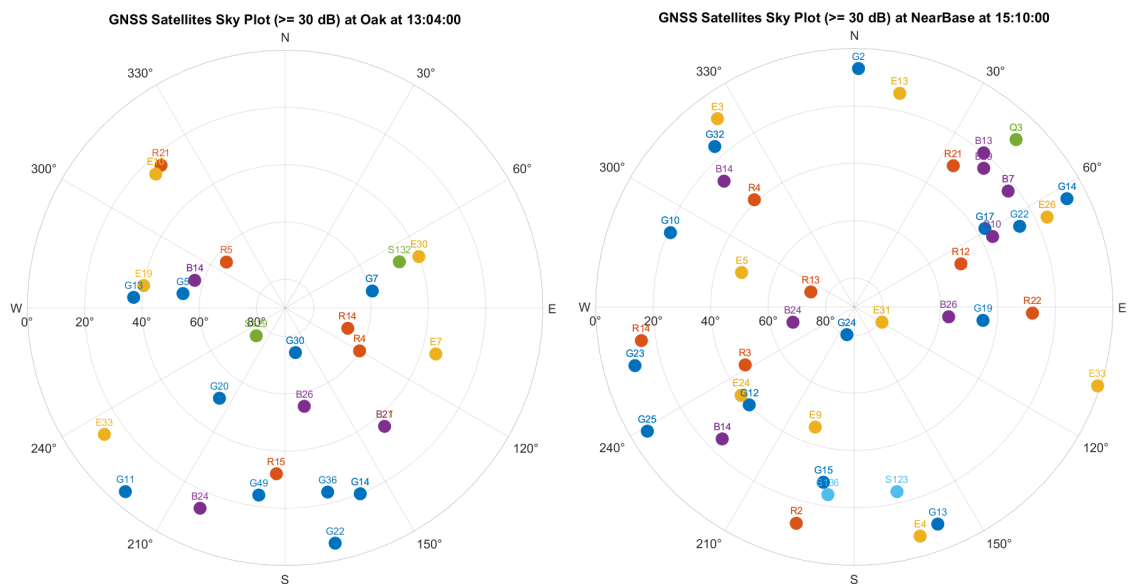


Figure B.3: Site Oak, Day 1 (left); Site Near Base, Day 2 (right).

B. Sky plot of GNSS satellites at each site

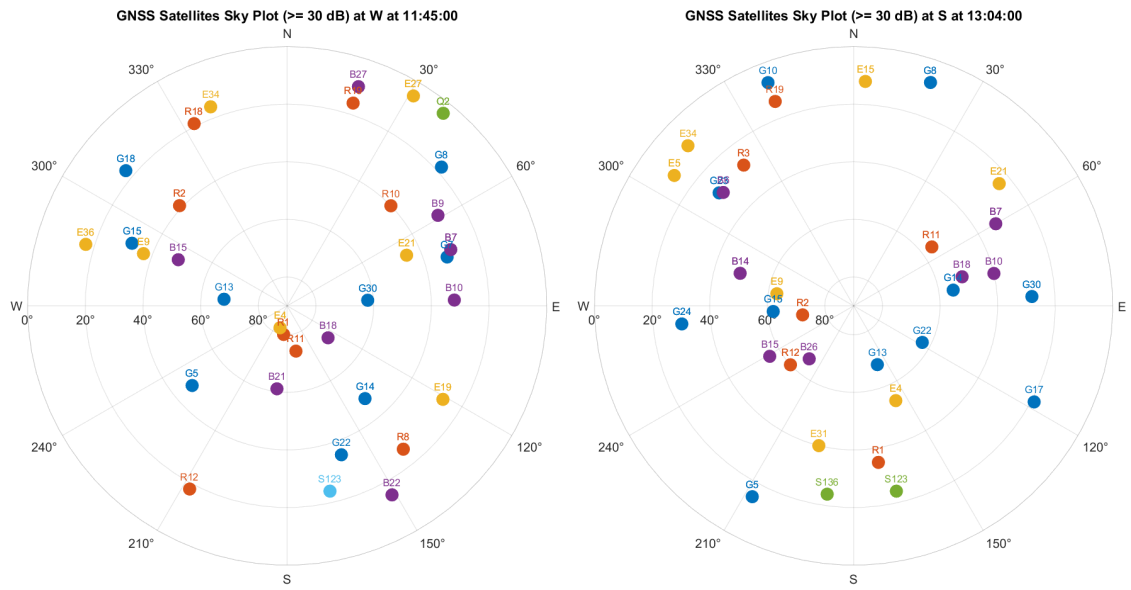


Figure B.4: Site W, Day 2 (left); Site S, Day 2 (right).

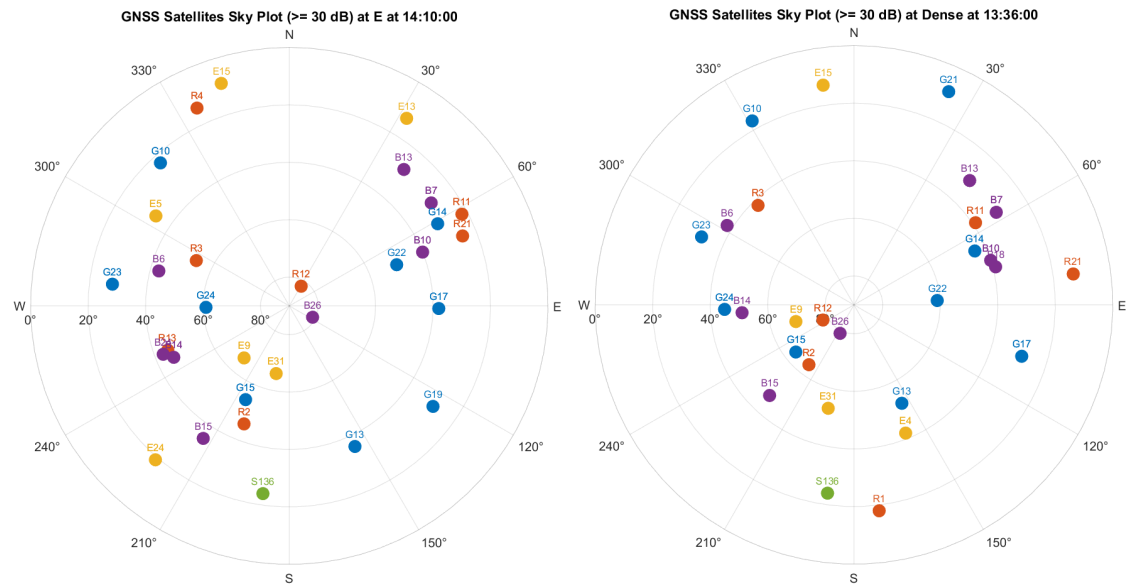


Figure B.5: Site E, Day 2 (left); Site Dense, Day 2 (right).

DEPARTMENT OF SPACE, EARTH AND ENVIRONMENT
CHALMERS UNIVERSITY OF TECHNOLOGY
Gothenburg, Sweden
www.chalmers.se



CHALMERS
UNIVERSITY OF TECHNOLOGY